Title:

Late Holocene seasonal temperature variability of the western Scottish shelf (St Kilda) recorded in fossil shells of the bivalve *Glycymeris glycymeris*

Authors:

Stella J. Alexandroff[a,b], Paul G. Butler[a], Philip R. Hollyman[c], Bernd R. Schöne[d], James D. Scourse[a]

Affiliations

[a]College of Life and Environmental Sciences, Exeter University, TR10 9EZ Penryn, United Kingdom,
[b]School of Ocean Sciences, Bangor University, LL59 5AB Menai Bridge, United Kingdom
[c]British Antarctic Survey, High Cross, Madingley Road, Cambridge, CB3 0ET, UK
[d]Institute of Geosciences, University of Mainz, Johann-Joachim-Becher-Weg 21, 55128 Mainz, Germany

Email addresses

Stella J. Alexandroff: s.alexandroff@exeter.ac.uk (corresponding author)
Paul G. Butler: p.butler@exeter.ac.uk
Philip R. Hollyman: phyman@bas.ac.uk
Bernd R. Schöne: schoeneb@uni-mainz.de
James D. Scourse: j.scourse@exeter.ac.uk

Keywords:

Sclerochronology; late Holocene; *Glycymeris glycymeris*; bivalve; sea surface temperatures; North Atlantic

Abstract

The North Atlantic Ocean and adjacent shelf seas play a crucial role in global climate. To better constrain long-term natural variability and marine-terrestrial linkages in this region, a network of highly resolved marine archives from the open ocean and continental shelves is needed. In recent decades, bivalve sclerochronology has emerged as a field providing such records from the mid- to high latitudes. In May 2014, dead valves and young live specimens of the bivalve *Glycymeris glycymeris* were collected at St Kilda, Scotland. A floating chronology spanning 187 years was constructed with fossil shells and radiocarbon dated to 3910–3340 cal yr before present (BP), with a probability density cluster at ca. 3700–3500 cal yr BP. Sub-annual $\delta^{18}O$ data were obtained from five fossil and three modern specimens and showed a strong seasonal signal in both time intervals. The growth season of *G. glycymeris* at this location today lasts from May to October, with most growth occurring before the temperature peak in August. Thus, the modern specimens and the fossil chronology represent late spring and summer sea surface temperatures (SST). The annual temperature range was 4.4 °C in the fossil shells, which is similar to the range observed today (3.8 °C). Average SSTs reconstructed from the fossil shells were 1 °C cooler than in 2003–2013 CE and similar to the early 20th century CE. The radiocarbon age of the floating chronology coincides with a climatic shift to wetter conditions on the British Isles and with a cold interval observed in palaeoceanographic records from south of Iceland. However, our data do not provide evidence of a cold interval on the Scottish shelf. The similarity in growth season and temperature range between the fossil and modern specimens are attributed to similar boundary conditions in the fourth millennium BP compared to today.

Graphical abstract

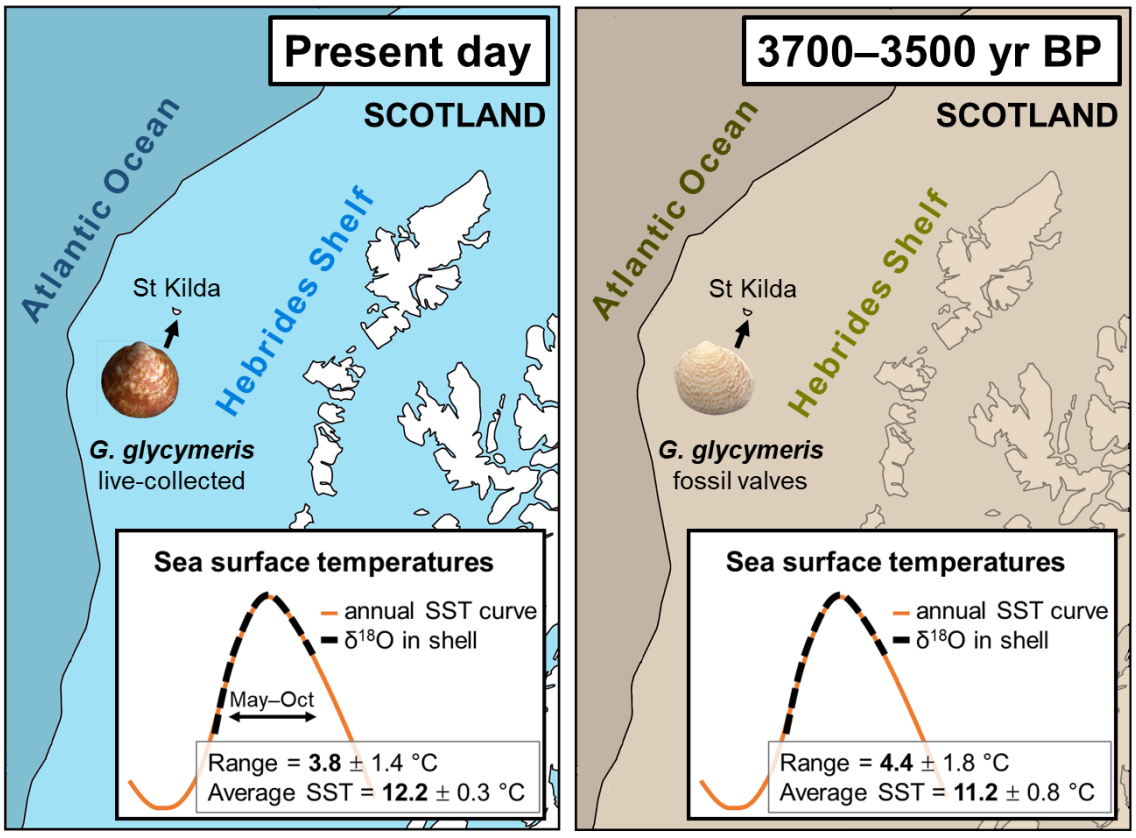

1. Introduction

The North Atlantic is a key region in the global climate system. The Atlantic Meridional Overturning Circulation (AMOC) plays a crucial role in the global redistribution of heat, carbon, and nutrients, and has been implicated in abrupt climatic shifts (Buckley and Marshall, 2015). In addition to the main North Atlantic basin, shelf seas are an integral part of the North Atlantic region. Shelf seas are in exchange with the open ocean, and disproportionately important for primary production and the sequestration of atmospheric carbon (Chen et al., 2013). Thus, understanding the dynamics and natural variability of the Atlantic circulation and adjacent shelf seas is crucial to understanding past and future climate changes.

North Atlantic sea surface temperatures (SST) have been decreasing since 5700 years before present (BP), which is generally linked to an orbitally forced decrease in solar irradiance (e.g., Marchal et al., 2002). However, SST trends and variability in the late Holocene are temporally and spatially heterogenous, due to processes in the different limbs of the AMOC and regional ocean-atmosphere feedbacks (e.g., Moffa-Sánchez et al., 2014; Solignac et al., 2008). In the fourth millennium BP, solar activity was relatively low, with a strong negative excursion noted at ca. 3.4 cal kyr BP (Steinhilber et al., 2012, 2009). The atmospheric conditions in the fourth millennium BP are thought to have been dominated by a weakly positive North Atlantic Oscillation (NAO) with several negative phases (Goslin et al., 2018; Olsen et al., 2012; Orme et al., 2017). A low-to-negative NAO is associated with a southward-shifted storm track and a southward-shifted and weaker North Atlantic Current (NAC; Curry and McCartney, 2001; Taylor and Stephens, 1998). However, reconstructed long-term trends of the NAO and storm track positions cannot provide a full picture of their high-frequency variability. For example, aeolian sediment reconstructions from the Outer Hebrides, Scotland, indicate strong westerly wind activity at ca. 3.3 cal kyr BP (Gilbertson et al., 1999; Orme et al., 2016), which could have caused increased Atlantic inflow on the Hebrides Shelf.

Traditional palaeoceanographic studies have mainly focussed on changes over millennia (Lynch-Stieglitz et al., 2007). However, instrumental observations of the AMOC show pronounced changes in the system on decadal scales (Robson et al., 2014). Thus, a dense network of proxies for past high-frequency variability of the AMOC is required to complement existing records of past climatic changes and to build a bridge to modern observations (Ninnemann and Thornalley, 2016). Moreover, hydroclimatic variability of the British Isles in the late Holocene has predominantly occurred on the decadal-to-centennial scale, with strong links to changes in North Atlantic ocean circulation (Charman, 2010; Swindles et al., 2013). While terrestrial records tend to be more highly

resolved due to fast sedimentation rates, marine records of equivalent resolution are rather scarce (Charman and McCarroll, 2010). Hence, to investigate and constrain marine-terrestrial relationships further, highly resolved marine records are needed; records from shelf seas are of particular interest as they are more tightly coupled with the adjacent terrestrial environment.

In recent decades, bivalve sclerochronology has emerged as a new research field with important applications in the study of highly resolved past marine variability (e.g., Jones, 1983; Schöne et al., 2005). The annual growth increments in long-lived bivalves reflect the environment the animals live in and can be crossmatched between specimens to construct multi-centennial chronologies (e.g., Butler et al., 2013). When live-collected specimens are incorporated into a chronology, the absolute calendar year of each annual increment is known and, through accurate crossmatching, dating uncertainties within the record can be virtually eliminated (Black et al., 2019). However, when working with fossil shells, it is not always possible to incorporate live-collected specimens into the chronology. Instead, crossmatched fossil shells build a 'floating chronology', which is not anchored in time (Scourse et al., 2006). While this means that floating chronologies do not provide absolute calendar dates, the growth records are annually resolved and, most importantly, replicated. Thus, floating chronologies provide valuable and robust high-resolution records of past environmental variability.

Previous studies have demonstrated that the long-lived bivalve *Glycymeris glycymeris* is a potential target for reconstructing climate variability in the North Atlantic region (Brocas et al., 2013; Featherstone et al., 2020; Reynolds et al., 2013; Royer et al., 2013). *G. glycymeris* can live for almost 200 years (Reynolds et al., 2013) as a shallow burrower in preferably coarse sediment like gravel or gravelly sand at depths up to 100 m (Thomas, 1975, and references therein). Shell growth occurs synchronously among specimens and populations that are exposed to the same environmental factors, which renders sclerochronological studies possible (Brocas et al., 2013; Reynolds et al., 2013). The growth increments are delimited by organic-rich growth lines that are formed each year when shell growth slows down drastically shortly after the temperature peak (e.g., Reynolds et al., 2017). Whether shell growth continues at a very slow rate throughout this 'off season' or ceases completely at one point is not known, but any information that might be stored in the annual growth lines is inaccessible to current sampling techniques. Consequently, 'annual' *G. glycymeris* growth records do not represent the entire year, but are instead biased towards the warmer months of the year. This seasonal bias is a common characteristic of bivalve chronologies at mid- to high latitudes (Killam and Clapham, 2018), and is usually regarded as a limitation. However, many climatic patterns and shifts result from processes that are also seasonally biased (e.g. seasonal flux of solar energy), and annual

averages of past climatic and environmental conditions mask such seasonal-scale variability (Carré and Cheddadi, 2017). Thus, seasonal bias in the growth record can potentially be used as an asset when the exact timing of the growth season is known. The growth season can be determined through sub-annual oxygen isotope samples of the shell carbonate ($\delta^{18}O_c$), which are calibrated against instrumental temperature records (e.g., Weidman et al., 1994). Furthermore, the sub-annual $\delta^{18}O_c$ series can provide insight into inter-annual variability of the respective growth season through time (Schöne and Fiebig, 2009; Wanamaker et al., 2011)

Here, we present a floating, crossmatched *G. glycymeris* chronology and associated sub-annual $\delta^{18}O_c$ profiles from the Hebrides Shelf, NW Scotland, radiocarbon dated to the fourth millennium BP. The fossil $\delta^{18}O_c$ series are compared to those of modern specimens from the same sample site. The aim of this study is to investigate seasonality and seawater temperatures on the Hebrides Shelf in the late Holocene and, in so doing, add to existing data on past marine variability in the Northeast Atlantic.

2. Geographical setting

2.1 The Hebrides Shelf

The Hebrides Shelf is located to the west of Scotland; the shelf edge extends from ca. 56° N to 60° N. The shelf slopes gently to the west of the Outer Hebrides until a water depth of 120–140 m is reached in the vicinity of the archipelago of St Kilda (Sutherland et al., 1984). The shelf edge is steep; to the west of the edge lies the Rockall Trough, which reaches depths of 2,000 m at this latitude (Holliday et al., 2000).

The shelf sea is influenced by Atlantic waters through shelf-ocean exchange, as well as by coastal waters through the Scottish Coastal Current (SCC). The SCC is a buoyant current that flows out of the Irish Sea through the North Channel (Fig. 1), carrying a mixture of relatively fresh Irish Sea and Clyde Sea waters and potentially influencing the entire western Scottish shelf (Ellett and Edwards, 1983; Inall et al., 2009, and references therein). The main component in the exchange between the Hebrides Shelf and the open ocean is the slope current (Fig. 1), a northwards-flowing current carrying nutrient-rich Atlantic water. The slope current is of the same origins as the upper waters in the eastern Rockall Trough and mainly consists of warm and saline Eastern North Atlantic Water originating from the south, which is then mixed with the cooler and fresher North Atlantic Current water. The interannual variability of temperature and salinity in the upper layers of the Rockall Trough is influenced by a dynamic system of different atmospheric and oceanic indicators, of

which the exact driving and forcing mechanisms have yet to be disentangled (Hughes et al., 2012). It is, however, evident that the strength of the Subpolar Gyre (SPG) plays an important role in the hydrographic variability of the Rockall Trough (Holliday, 2003; Holliday et al., 2008; Hughes et al., 2012). A strong SPG circulation is thought to increase inflow of fresh and cool Atlantic water, whereas a weak SPG results in warmer and more saline upper waters (e.g., Hátún et al., 2005; but see Foukal and Lozier, 2017).

Water mass exchange between the ocean and the continental shelf is facilitated through seasonal and topographical "weak points" in the slope current, which allow Atlantic water to flow onto the shelf (Pingree et al., 1999). Firstly, while the current is the strongest in winter, the poleward flow becomes weaker in other seasons, and might even be reversed (i.e. equator-ward) in the early spring (Pingree et al., 1999). Secondly, abrupt topographical changes in the slope lead to a breakdown of the insulation, allowing oceanic water to intrude onto the shelf (Pingree et al., 1999). Most importantly, the slope current itself is an integral part of the shelf-ocean exchange through wind-driven on-shelf transport of oceanic surface water and off-shelf transport of deep shelf water through downwelling processes known as Ekman drains (Holt et al., 2009; Simpson and McCandliss, 2013; Souza et al., 2001), as well as through winter cascades (Shapiro et al., 2003; Shapiro and Hill, 1997). Most recently, the inflow of slope current water onto the shelf at ca. 55.4° N has been identified as a distinct current, called Atlantic Inflow Current (AIC; Fig. 1; Porter et al., 2018). The AIC transports nutrient-rich slope current water onto the shelf, where it mixes with the fresher and cool Irish Coastal Current (Fig. 1b) flowing northwards (Porter et al., 2018).

The Northwest European Continental shelf plays an important role as a carbon sink by fixing atmospheric CO_2 and transporting it to deep layers of the open ocean through downwelling processes (Chen et al., 2013; Simpson and McCandliss, 2013). Painter et al. (2016) studied the carbon exchange between the open ocean and the Hebrides Shelf and found a net off-shelf transport of particular organic carbon, with fluxes that are three to five times larger than the global mean.

2.2 St Kilda

St Kilda is an isolated volcanic archipelago on the Hebrides Shelf (Lat: 57.82° N, Long: 08.59° W, Fig. 1). It forms the westernmost point of the Outer Hebrides, Scotland, and is located 64 km west-northwest of the nearest inhabited land, North Uist. It is thus an offshore environment largely unaffected by terrestrial freshwater input. The archipelago consists of four major islands, of which Hirta is the biggest one with a circumference of 14 km, and several rock stacks.

The cliff line of St Kilda today plunges steeply into the sea until it is interrupted by a platform with several sub-surfaces and steps between 40 m and 80 m depth. These surfaces are thought to have

been formed about 12,600–11,500 years ago, during the abrupt cooling of the Younger Dryas or Loch Lomond Stadial (Sutherland et al., 1984). At 120 m below the current sea level, another platform is present, which was most likely formed during the Last Glacial Maximum about 22–19 kyr ago (Sutherland et al., 1984). The surrounding shelf to the north, west, and south is marginally deeper (up to 140 m) than the lowest platform, while it gradually shoals to the east.

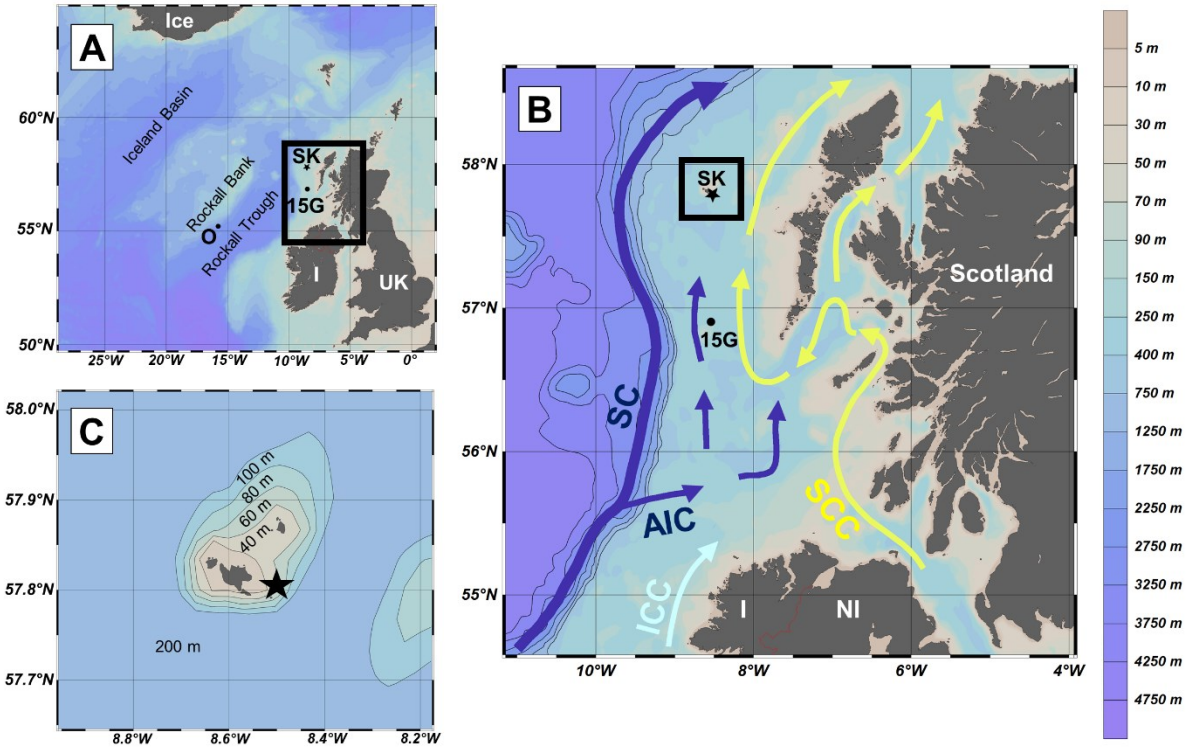

Figure 1: Location of the sample site at St Kilda, Scotland. **(A)** Overview map. Colours indicate bathymetry according to the legend to the right. Land masses are labelled with "Ice" = Iceland, "I" = Ireland, "UK" = United Kingdom. "15G" = Ellett line station 15G, marked with a dot. "O" = Location of $\delta^{18}O_w$ measurement (Östlund and Grall, 2001) referred to in section 3.6.3, marked with a dot. The black rectangle indicates the location of the detail shown in map B. **(B)** Detail of map A. Sample location (black star) at St Kilda, Outer Hebrides, Scotland. The yellow arrows indicate the approximate circulation of the Scottish Coastal Current (SCC). The dark blue arrows indicate the flow of the slope current (SC) and Atlantic Inflow Current (AIC) transporting Atlantic water. The light blue arrow indicates the Irish Coastal Current (ICC). Background colours indicate bathymetry according to the legend to the right. Depth contours for the shelf margin and open ocean are drawn in black lines. The shelf margin is denoted through depth contours starting from 200 m. Approximate positions of currents were taken from Inall et al. (2009), Turrell et al. (1996), and Porter et al. (2018). Land masses are labelled with "Scotland", "I" = Ireland, and "NI" = Northern Ireland. The black rectangle indicates the location of the detail in map C. **(C)** Detail of map B. Shown is the archipelago of St Kilda with the surrounding bathymetry. The respective depths are indicated within each depth contour line. The black star marks the sample site of this study. (Ocean Data View; Schlitzer, 2020)

Even though the St Kilda archipelago is located on the European shelf, it topographically approaches an ideal isolated island (Simpson and Tett, 1986). Simpson and Tett (1986) reported that

cold-water upwelling at St Kilda results in an increase in water column phytoplankton production of 40 % over an area of 5,000 km^3. This phenomenon of observed increase in primary production around islands is called 'island mass effect' (Doty and Oguri, 1956). The mixing caused by St Kilda has an important effect on the food chain beyond the local ecosystem, including large regions of spawning and nursery grounds for fish (Ellis et al., 2010).

3. Methods

3.1 Sample site and material

The material for this study was collected at Village Bay, St Kilda, during a research cruise aboard the RV *Prince Madog* in May 2014 (Lat: 57.80° N, Long: 08.55° W; Fig. 1). Apart from seven young live *G. glycymeris* specimens, most of the material consisted of single *G. glycymeris* valves (n = 645). All samples were collected at 40–65 m depth in parallel tows using a customised dredge of 1 m width (for a description see Butler et al., 2009b). The dead-collected samples presented in this paper were collected in two neighbouring tows at 46–65 m depth. The live-collected samples were collected in three different tows at 48–65 m depth.

3.2 Sample preparation

Specimens were preselected based on their suitability for sclerochronological studies; e.g. they should be expected to present more than 30 annual increments, not too heavily eroded, and with either hinge plate or shell margin or both still intact. Crossmatching was carried out using magnified images taken from acetate peel replicas of the acid-etched surface of sectioned shells as described by Kennish et al. (1980) and Ropes (1987). A summary of the steps is given below.

Specimens selected for processing were first measured and weighed. Given that *G. glycymeris* are equivalved (i.e. symmetrical along the hinge line), we can exclude the possibility that two valves of significantly different length, shape, and mass stem from the same individual. We used this observation to exclude the possibility of accidentally cross-matching two valves of the same specimen. The shells were then embedded in polyester resin and sectioned along the axis of maximum growth with a low-speed precision saw equipped with a diamond blade of 0.9 mm thickness. The sectioned blocks were then ground, polished, rinsed, and left to dry. Once dry, the blocks were etched to enhance the contrast between annual growth increments and the organic-rich growth lines as the latter form etch-resistant ridges (Goodwin et al., 2001; Schöne et al., 2002). Etching also enhances other patterns in the shell, such as the crossed-lamellar microstructures and microtubuli that are

present in *G. glycymeris* shells (Crippa, 2013), which in turn may obstruct the annual lines (pers. observation). Given that the annual growth lines in the fossil shells were not as clear as those in the modern shells, they were more prone to being masked by other patterns in the shell. Therefore, the fossil shells had to be etched in a weaker acid. After some trial and error, the modern shells were etched in 0.1 M hydrochloric acid (HCl) for 1.5 min, while the fossil shells were etched in 0.01 M HCl for 40 min. The etched, dry surface was then coated with ethyl acetate and covered with a cellulose acetate sheet to produce a replicate for photographic imaging.

The acetate peels were photographed using a Meiji MT8100 microscope in combination with a Lumenera Infinity 3 microscope camera and the software ImagePro Premier 9.1. The increment widths were measured based on photographs of the hinge plate (5x magnification), where growth patterns are much clearer than in the margin in *G. glycymeris* shells (pers. observation).

3.3 Crossmatching and chronology construction

Correlations between the shells were visualised and quantified using the MATLAB script SHELLCORR (written by Ian Harris, UEA; Scourse et al., 2006). A detailed description of SHELLCORR is given in Scourse et al. (2006) and Butler et al. (2009a). Once the seven shells presented here were successfully crossmatched, a master chronology was built using the dendrochronology programme ARSTAN (Cook, 1985; Cook and Krusic, 2005). ARSTAN detrending removes the ontogenetic and geometrical growth trends and creates growth indices of each series with a mean value of 1. The raw series were power-transformed, detrended by fitting a negative exponential curve, and stacked in a chronology using a bi-weight robust mean function (Cook et al., 1990).

The quality of the chronology was quantified using the series inter-correlation (Rbar) and the expressed population signal (EPS; Wigley et al., 1984). The Rbar measures the mean correlation between all detrended series, and thus the strength of the signal common to all time series in the chronology. The EPS measures how well the chronology signal represents the population signal and is calculated based on the Rbar and the number of series. Wigley et al. (1984) recommended a minimum EPS of 0.85 to ensure that the chronology provides a good enough representation of the population signal.

3.4 Radiocarbon dating

Six of the seven crossmatched specimens were radiocarbon dated with AMS. Four shell samples were sent to Beta Analytic, and two samples were later analysed at the ^{14}CHRONO Centre for Climate, the Environment and Chronology at the Queen's University in Belfast. All radiocarbon

dates were calibrated with Calib 7.1.0 (Stuiver and Reimer, 1993) using the MARINE13 calibration curve (Reimer et al., 2013). The calibration curve automatically applies an age-dependent, "global" average marine reservoir correction of approximately 400 ^{14}C yr based on the spatially averaged modelled value for the surface mixed layer of the ocean. In addition, we applied a regional ΔR correction of –33 ± 93 ^{14}C yr as recommended for the Scottish and Irish west coasts for the past 5900 years by Reimer et al. (2002).

To constrain dating uncertainties, the radiocarbon dates were "wiggle-matched" to the calibration curve using the Bayesian defined sequence model in OXCAL 4.3 (Bronk Ramsey et al., 2001; Bronk Ramsey, 2009). This has been undertaken in sclerochronological studies before, e.g. in an archaeological context (Helama and Hood, 2011). Here, the calibrated radiocarbon dates plus the known gaps between samples (i.e., the absolute number of years between the death of one specimen and that of another) were combined and fitted to the calibration curve to calculate a probability density for the age of each sample. MARINE13 was again chosen as the calibration curve.

3.5 Raman spectroscopy

Diagenesis of aragonite can alter the oxygen isotopic composition and thus impact palaeotemperature reconstructions (Cochran et al., 2010; Pederson et al., 2019; Urey et al., 1951). Raman spectroscopy can be used to distinguish between the different polymorphs of calcium carbonate, as it produces different spectra specific to each crystal structure (De La Pierre et al., 2014). In order to confirm that aragonite in the fossil shells had not been converted to calcite, micro-Raman spectroscopy was performed on fossil shell specimens at the Diamond Light Source, Oxford. A 473 nm laser at a power of 15 mW with a magnification of 20x was used for the analysis. Raman spectra were acquired from each visible shell layer; as all displayed coincident peaks only the spectra from the outermost shell layer are presented here. Spectra between 135 and 1100 cm-1 are described, as these wavelengths are used to distinguish between calcium carbonate polymorphs (Parker *et al*., 2010; Wehrmeister *et al*., 2010). Samples of known composition were also analysed for comparison of key interpretative bands (synthetic calcite and speleothem aragonite, Brinza et al. 2014).

3.6 Stable isotope sampling

G. glycymeris shells consist of an inner shell layer (ISL) and an outer shell layer consisting of simple crossed lamellae (Crippa, 2013). The outer shell layer can be further divided into an inner portion (iOSL) and an outer portion (oOSL, Fig. 2). While the iOSL and oOSL are not distinct layers, they exhibit different patterns of the first order elements in the simple crossed lamellae (Crippa, 2013). As isotopic fractionation differs between the iOSL and oOSL in *G. glycymeris* (pers.

observation; see Trofimova et al. (2018) for a relevant study of *A. islandica*), it is important to remove the samples from the same portion of the outer layer. All samples in this study were taken in the oOSL.

Shell carbonate powder was extracted through microdrilling and micromilling (Dettman and Lohmann, 1995) and analysed using continuous-flow isotope ratio mass spectrometry (CF-IRMS; see below).

The samples were mainly microdrilled using an ESI New Wave robotic micromill fitted with an Olympus SZ61 camera and loaded with a 300 µm drill bit (Fig. 2, "DR"). Three individual increments were also micromilled horizontally in a mirror section of specimen VB132 (Fig. 2, "SM"), allowing for direct comparison between the two methods in the same shell. Microdrilling provided a sample resolution of 300 µm (i.e. the diameter of the drill bit), and each sample spot was adjacent to the next spot, without overlapping. Micromilling provided a sample resolution of 150 µm. Both fossil and modern specimens were microdrilled in the 8–11 widest (i.e. ontogenetically youngest) increments of the shell margin.

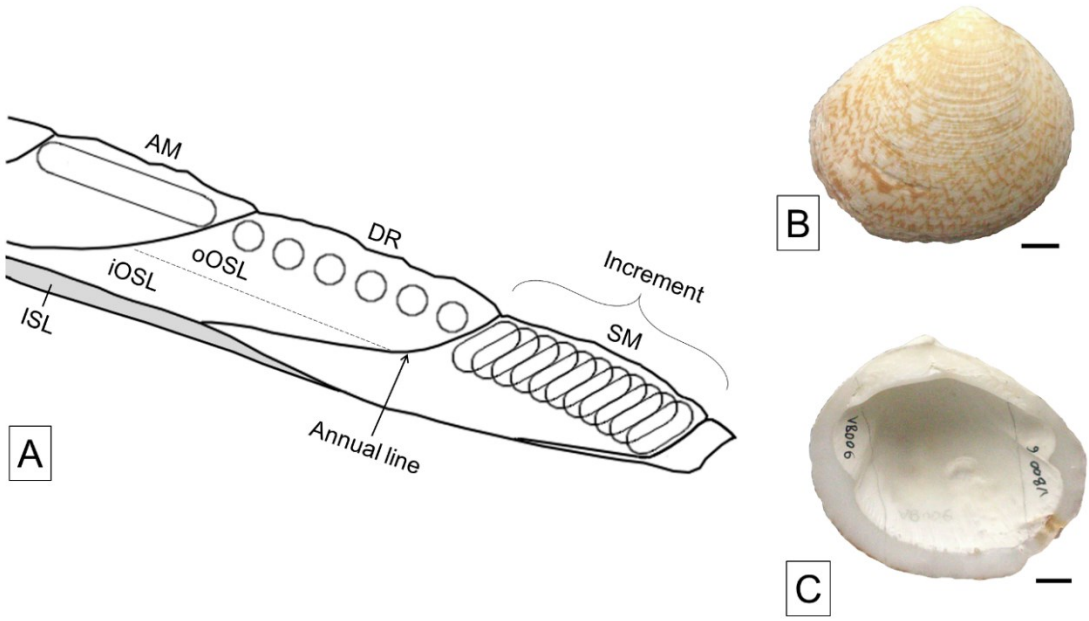

Figure 2: (A) Different sampling techniques. AM = Annual micromilling (not used here), DR = Microdrilling, SM = Sub-annual micromilling. oOSL = Outer portion of the outer shell layer; iOSL = Inner portion of the outer shell layer; ISL = Inner shell layer. The annual line is indicated by an arrow. Increment = portion between two annual lines. **(B)** Fossil specimen VB006 (outside). **(C)** Fossil specimen VB006 (inside). Scale bars indicate 1 cm.

Shell powders (ca. 70 µg) were digested in He-flushed borosilicate exetainers at 72 °C with water-free phosphoric acid for 2 hours and the liberated CO_2 gas was measured in a ThermoFisher MAT 253 CF-IRMS coupled to a GasBench II at the University of Mainz. Stable oxygen isotope values are reported

in δ-notation and given in parts per mil (‰). Data were calibrated against an NBS-19 calibrated Carrara Marble distributed by IVA Analysentechnik GmbH & Co. KG ($\delta^{18}O$ = −1.91 ‰). The long-term 1σ accuracy (based on 421 blindly measured NBS-19 samples) and the average 1σ internal precision of the samples were better than 0.04 % and 0.07 ‰, respectively. No correction was applied for differences in acid fractionation factors of the reference material (calcite) and shells (aragonite), because the palaeothermometry equation used below (Eq. 1) also did not consider these differences (Füllenbach et al., 2015). However, a correction of −0.38 ‰ would be required if $\delta^{18}O$ values of shells and other carbonates were compared with each other.

3.6.1 Modern oxygen isotope samples

The positions of the annual lines within the oxygen isotope ($\delta^{18}O_c$) series were identified visually by analysing microscope pictures obtained through the methods described in section 3.2. The series were converted into seawater temperatures (see below). Then, each annual peak in the $\delta^{18}O_c$-derived temperature series was aligned with the peak in the corresponding calendar year of the Met Office HadISST 1.1 data (Rayner et al., 2003) for the 1x1-degree grid cell covering St Kilda (57–58 °N, 8–9 °W) using AnalySeries 2.0.8 (Paillard et al., 1996). All data points to the left and to the right of each peak were fit to the remaining temperature series.

3.6.2 Palaeotemperature equation

Seawater temperatures were obtained from the $\delta^{18}O_c$ series using the palaeotemperature equation developed by Grossman and Ku (1986) with a PDB-VMOW scale correction of −0.27 ‰ (Dettman et al., 1999; Gonfiantini et al., 1995; Hut, 1987) for:

$$T\,°C = 20.6 - 4.34\,(\delta^{18}O_{ar} - (\delta^{18}O_w - 0.27)) \quad (1),$$

where $\delta^{18}O_{ar}$ is the $\delta^{18}O$ of shell aragonite relative to VPDB, and $\delta^{18}O_w$ is the $\delta^{18}O$ of the water relative to VSMOW.

As no local $\delta^{18}O_w$ values are available for St Kilda, the NASA Global Seawater Oxygen-18 Database (https://data.giss.nasa.gov/o18data/) was used to find the closest available value. One of the closest locations where $\delta^{18}O_w$ has been measured is at 55.3 °N 15.6 °W (Östlund and Grall, 2001; see Figure 1a, point "O"), where the value is 0.38 ‰. We chose this location because the measurement was taken at a similar depth (46 m) to our sample depth, and it represents an offshore environment in

365 the Rockall Trough area. In this study, it was assumed that $\delta^{18}O_w$ has remained constant over the last
366 four millennia at our sample site, and thus 0.38 ‰ was used for all time intervals.

367

368 **3.6.3 Seasonality**

369 Alignment of isotope series and instrumental data was done with the age-depth correlation
370 tool in AnalySeries 2.0.8 (Paillard et al., 1996). For comparison of seasonality between the modern
371 and the fossil series, all isotope series were first detrended and then resampled (see Schöne and
372 Fiebig, 2009; Wanamaker et al., 2011): Following the methods used by Wanamaker et al. (2011), a
373 linear regression model was fitted to each isotope series to calculate the low-frequency trend, and the
374 trend was subtracted from the raw $\delta^{18}O_c$ values. The mean $\delta^{18}O_c$ value was then removed from each
375 isotope series (i.e. each shell). The resulting normalised series were divided into individual years (i.e.
376 shell increments) for resampling. This resampling corrects the bias introduced by sampling increments
377 from different ontogenetic stages with different growth rates. Wanamaker et al. (2011) detrended and
378 resampled all increments with seven or more samples using a 7-point model, arguing that it would still
379 account for the annual seawater temperature cycle. In the present study, a 6-point model was used
380 instead, as a higher number than six would exclude all increments with six or fewer sample spots, and
381 thus leave too few for analysis. All increments with more than six oxygen isotope values were fitted
382 to a cubic spline model and downsampled to six samples per increment using the fitting tool in
383 AnalySeries 2.0.8.

384 Downsampling the data to fit a 6-point model might attenuate the signal and decrease the
385 temperature range captured by $\delta^{18}O_c$. Therefore, the results were scaled to allow meaningful
386 comparisons between time periods. Following the methods described by Wanamaker et al. (2011), a
387 scaling factor was calculated based on the temperature range difference between modern *G.*
388 *glycymeris* samples and instrumental data, and then applied to the fossil shell records.

389

390 **3.6.4 Average temperatures**

391 To obtain comparable mean temperatures for each time interval, the $\delta^{18}O_c$ series were again
392 resampled by fitting them to a 6-point cubic spline model (see section 3.6.4), this time without
393 detrending the data. The same shells were used as in the section above, and again only increments
394 with six or more isotope samples were considered.

395

396

397

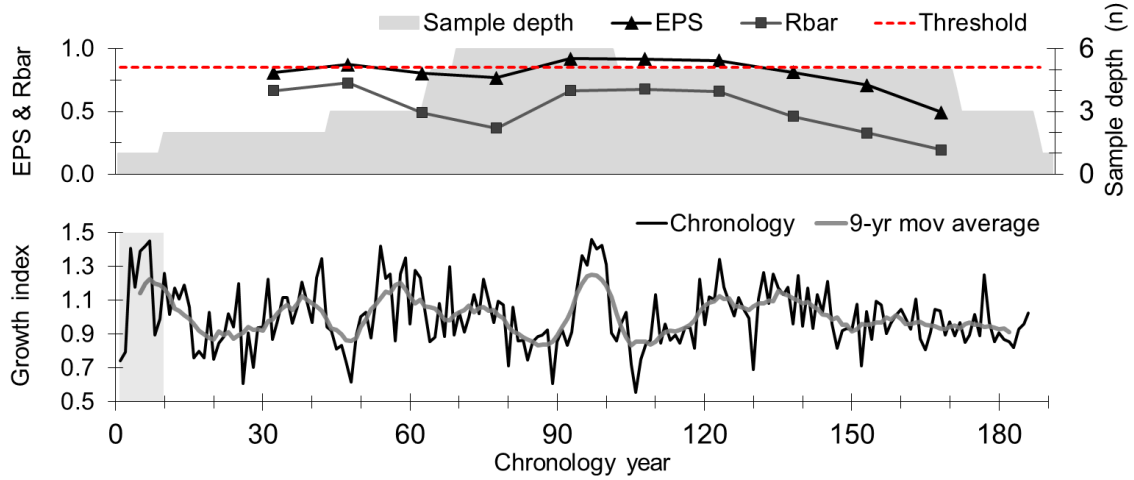

Figure 3: Late Holocene floating chronology. The top panel shows sample depth, EPS and Rbar of the chronology. The red dashed line is the 0.85 EPS threshold as suggested by Wigley et al. (1984). The bottom panel shows the standardised annual growth indices (black line) and a 9-year moving average (grey line). The first ten years of the chronology consist only of one specimen and are shaded grey.

4. Results

4.1 Floating chronology

The floating chronology was constructed with seven dead-collected *G. glycymeris* from St Kilda. Because this chronology is not absolutely dated, the time axes are reported in chronology years (Fig. 3).

The increments of the hinge plate in the first 10–20 ontogenetic years were narrow and often contained the spurious lines sometimes known as "doublets" (Butler et al., 2009a), which complicated crossmatching. Thus, the first 20 years of each specimen were excluded from further analysis. The resulting chronology consists of seven shells and spans 187 years (Fig. 3).

The first ten years of the chronology include the growth indices of only one specimen and should thus be treated with caution. The chronology is statistically robust or close-to-robust for ca. 110 years, with an EPS above 0.85, apart from a short period at around year 80 where the EPS dips below 0.80 (Fig. 3). The EPS and Rbar decrease towards the end of the chronology, starting at around year 140. The mean interseries correlation of the chronology is 0.58.

417 **4.2 Radiocarbon dating**

418 Six specimens (i.e., all but VB023) of the fossil *St Kilda Seven* chronology were radiocarbon
419 dated, placing the chronology in the fourth millennium before present (BP = 1950). Dating
420 uncertainties were constrained with a Bayesian chronological model. The modelled dates range from
421 3910 to 3340 cal yr BP, which reduce the unmodelled range (3910–3230 cal yr BP) by 110 years
422 (Table 1; Fig. 4). The modelled probability densities show several peaks along the time axis (Fig. 4).

423

424 **4.3 Raman spectroscopy**

425 The fossil shells showed no signs of diagenesis, all Raman spectra of the fossil shells being
426 consistent with those of aragonite (Fig. 5). Clear characteristic aragonite peaks were identified at 153,
427 181, 206 and 702-706 cm^{-1} (Parker *et al*., 2010) along with a characteristic calcium carbonate peak at
428 1085 cm^{-1} (Wehrmeister *et al*., 2010). No characteristic calcite peaks were identified in any spectra
429 acquired from fossil *G. glycymeris*.

430

431 **Table 1**: Radiocarbon ages of the *fossil G. glycymeris* shells. The unmodelled and modelled calibrated ages with
432 a 95.4% probability (2-σ) are given after a local marine reservoir correction of $\Delta R = -33 \pm 93$ has been applied.
433 Calibrations were made using the MARINE13 calibration curve (Reimer et al., 2013). Modelled dates refer to
434 dates output by the chronological model (Bayesian tree-ring sequence model in OXCAL 4.3).

Specimen	Lab ID	Conventional ^{14}C age (yr BP)	2 σ (95%) calibrated age (cal yr BP)	Modelled age (cal yr BP)
VB003	Beta-408875	3650 ± 30	3840–3360	3910–3420
VB004	Beta-408876	3630 ± 30	3830–3350	3870–3380
VB006	UBA-29386	3700 ± 30	3910–3420	3840–3350
VB020	Beta-408878	3700 ± 30	3910–3410	3840–3350
VB021	UBA-29389	3550 ± 30	3720–3230	3820–3340
VB024	Beta-408879	3710 ± 30	3930–3430	3820–3340

435

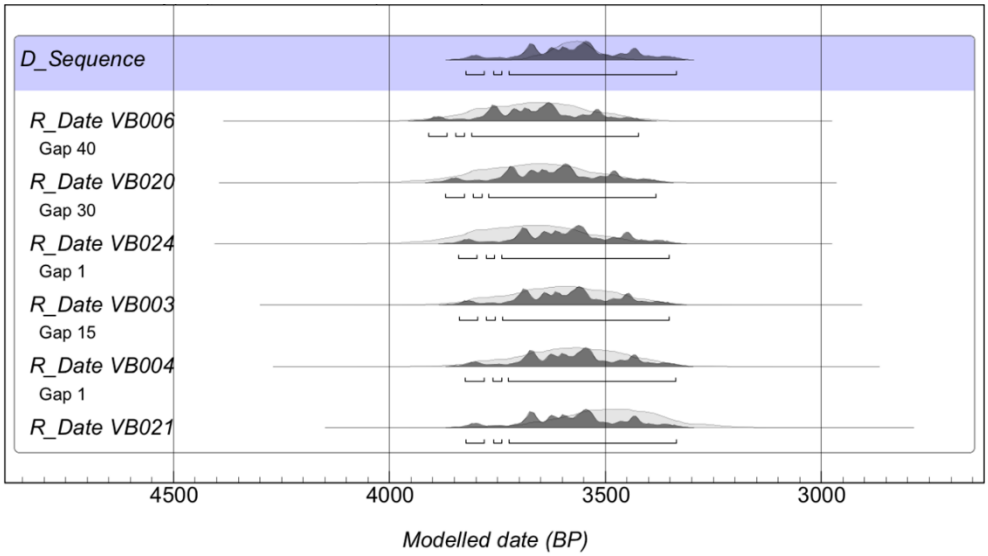

Figure 4: Probability densities of the death dates of six *St Kilda Seven* specimens and the combined series (D_Sequence), applying a ΔR correction of –33 ± 93. The sample IDs and offsets between each specimen as derived from crossmatching are given in the left column. The pale grey distribution curves represent the radiocarbon calibration probability distribution. The dark grey distribution curves are the resulting probability distributions obtained by the chronological model. The square brackets indicate a 95.4% probability. The top distribution curve (D_Sequence) is the result of wiggle-matching the crossmatched series to the radiocarbon calibration curve using the χ^2 test.

436

437

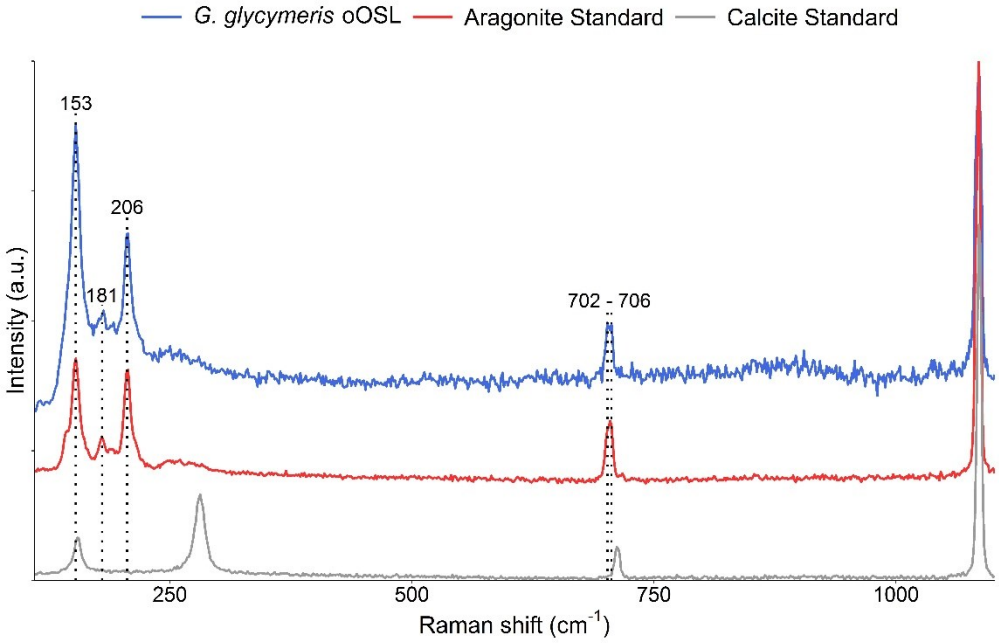

Figure 5: Raman spectra acquired between 135 and 1100 cm-1 for the oOSL of a fossil *G. glycymeris* along with spectra from speleothem aragonite and synthetic calcite. Characteristic peaks in the spectra are indicated (dotted lines) for coincident peaks in the shell and speleothem aragonite. A clear matching peak at 1085 cm^{-1} is visible for all samples. The y-axis is displayed as arbitrary units of intensity.

438

4.4 Oxygen isotopes

Oxygen isotope values are presented for three live-collected shells (2005–2013 CE) and five fossil shells from the floating chronology (3910–3340 cal yr BP). The three modern shells yielded sub-annual $\delta^{18}O_c$ for between 8 and 11 growth seasons (i.e. 'annual' increments) each and were averaged into one combined series spanning 2005–2013 CE. All seven fossil shells from the floating chronology were sampled; however, two shells (VB003 and VB024) were excluded from further analysis due to low sampling resolution. Figure 6 shows the position of each of the remaining five fossil $\delta^{18}O_c$ series in the floating chronology, which span between 11 and 14 growth seasons each. Specimens VB004 and VB021 were combined into one average series due to their overlap in time. Thus, there are four windows in the floating chronology: Two separate series at the beginning of the chronology (VB006, VB020), one combined series in the middle of the chronology (VB004 and VB021), and one series at around year 140 (VB023). All modern and fossil shells showed a clear seasonal signal (Fig. 7). The isotope series of the two coeval fossil specimens presented a warming trend (VB004 and VB021; Fig. 7).

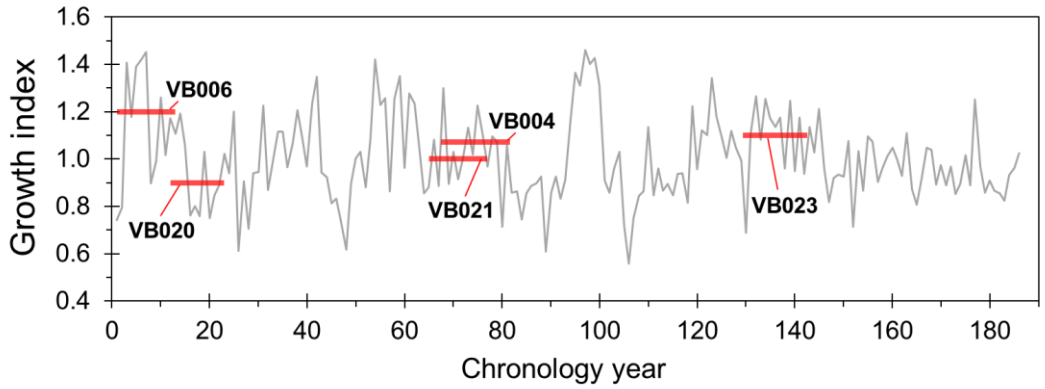

Figure 6: Positions of the fossil $\delta^{18}O_c$ series in the floating chronology.

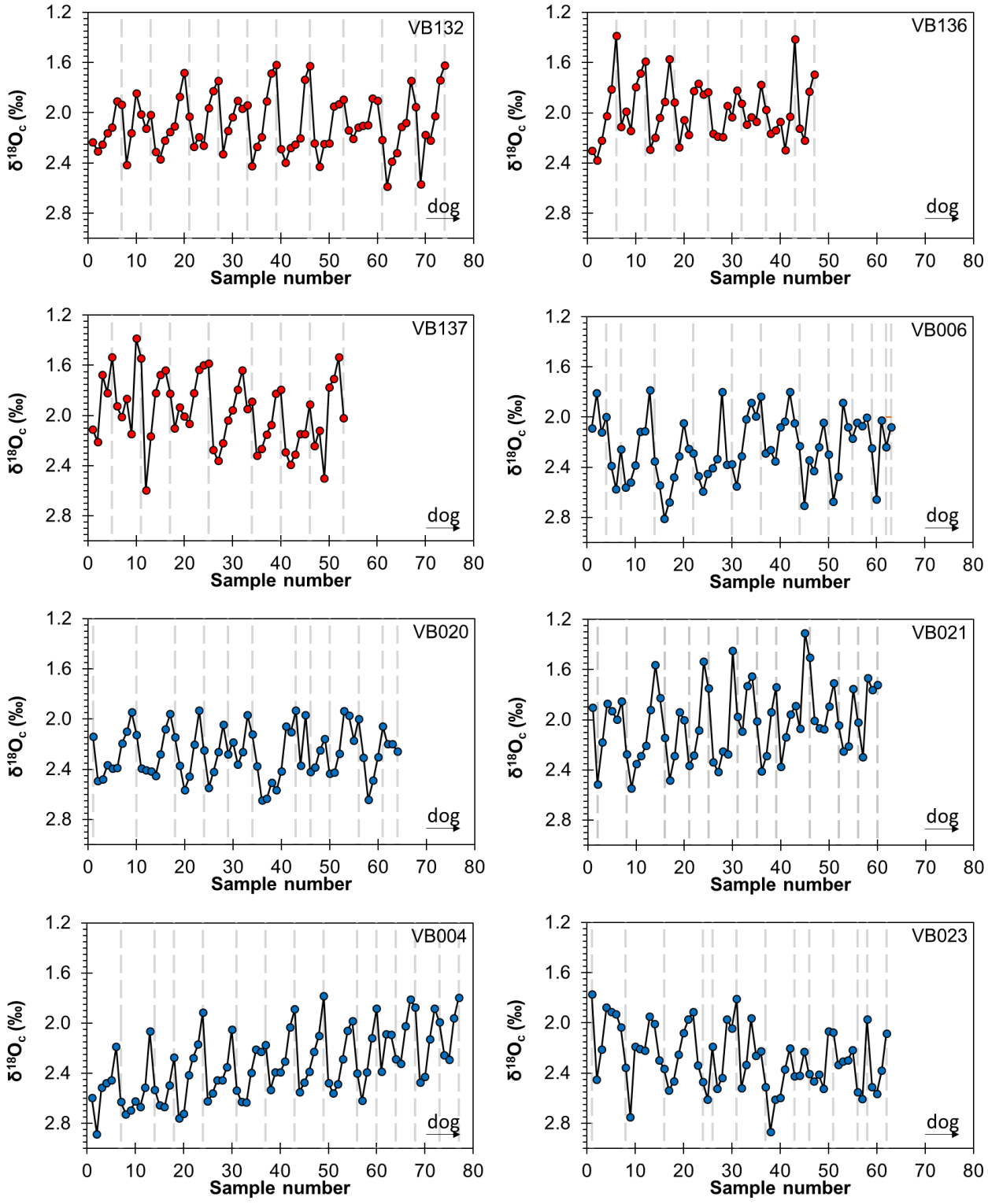

Figure 7: $\delta^{18}O_c$ values for the modern shells (red dots; VB132, VB136, VB137) and the fossil shells (blue dots; VB006, VB020, VB004, VB021, VB023). The sample direction followed the direction of growth (dog), from the ontogenetically youngest increments towards the more mature increments. The dashed vertical lines coincide with the last sample of each growth season. Note that the y-axes are inverted, thus, peaks in the plots correspond to temperature peaks. Each sample spot has a 300 µm diameter.

455

456

4.4.1 Modern oxygen isotope records compared to instrumental temperature data

Figure 8 shows the $\delta^{18}O_c$-derived seawater temperatures obtained by microdrilling, aligned with gridded sea surface temperatures for 2005–2013 CE. The two series are highly correlated. Figure 9 presents data from three calendar years (2008, 2011, 2012 CE), comparing the different sample techniques. These three years were chosen because they provided the best sampling resolution across all three specimens. All sample techniques yielded data that indicate a main growth season of *G. glycymeris* at St Kilda from May to September/October, with a bias towards the late spring and summer months (Fig. 9).

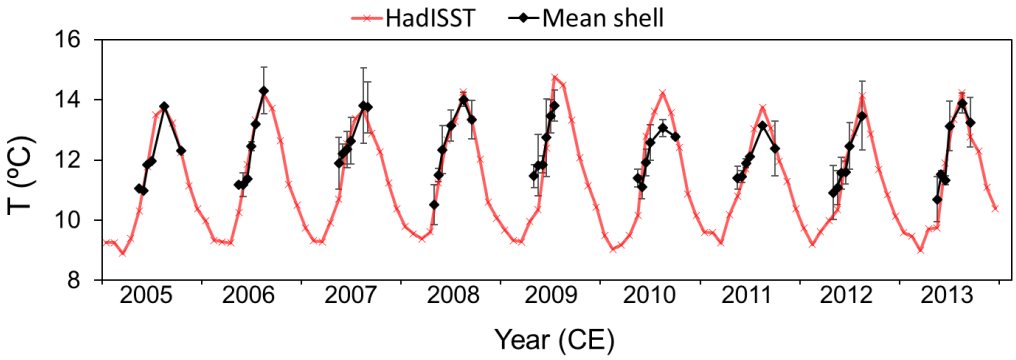

Figure 8: Average sub-annual temperature series derived from oxygen isotopes in three live-collected *G. glycymeris* shells (black line), compared to monthly gridded sea surface temperature data (HadISST1) for 2005–2013 CE. Error bars represent one standard deviation.

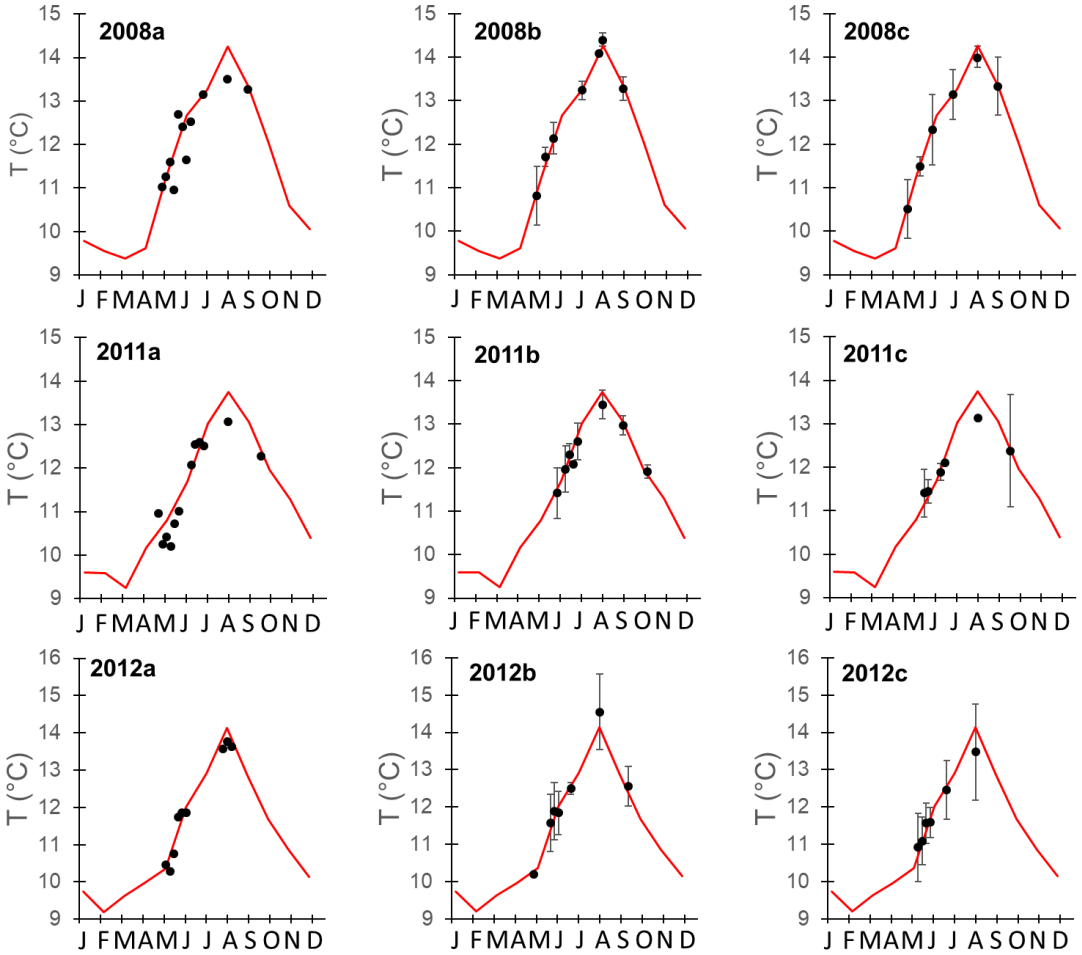

Figure 9: Sub-annual temperature series for 2008 CE (top row), 2011 CE (middle row), and 2012 CE (bottom row). Red line: Monthly HadISST1 data. Black dots: $\delta^{18}O_c$-derived seawater temperatures. The left column (a) shows micromilled samples from one specimen (VB132); the middle column (b) shows the combined series of three microdrilled specimens (same data as in Fig. 8); the right column (c) shows the average series of the resampled microdrilled samples after a cubic spline has been fitted. Error bars indicate one standard deviation. The corresponding months are given on the x-axis for each year, starting with J = January.

4.4.2 Comparison of modern and fossil data

The average range in $\delta^{18}O_c$ and the average reconstructed temperatures for the fossil and modern series are given in Table 2. The annual temperature range from May to October in 2003–2013 CE was $\Delta T = 3.8$ °C (calculated with HadISST1.1 data). The annual temperature range recorded in the resampled modern isotope series was 1.55 times smaller ($\Delta T = 2.5$ °C; Fig. 9c). Consequently, the $\delta^{18}O_c$-derived temperature ranges of both time periods (ca. 3.6 cal kyr BP and 2003–2013 CE)

were multiplied by the scaling factor of 1.55. The scaled seasonality was similar albeit slightly higher in the fossil shells compared to 2003–2013 CE (4.4 °C ± 1.8 °C; Table 2).

The average sea surface temperature (SST) recorded by the fossil shells was 11.2 °C ± 1.2 °C, whereas the modern shells yielded average SSTs of 12.2 °C ± 0.5 °C (Table 2).

Table 2: Average $\Delta\delta^{18}O_c$ and spring and summer seasonality (detrended values, left), and average $\delta^{18}O$ and derived average temperatures per time period for the annual growth season (undetrended values, right). Individual series of the floating chronology are shown in the top four rows, as well as the mean value for the floating chronology (3.6 kyr BP avr) and for the combined series of the live-caught shells (2003-2013 CE). $\Delta\delta^{18}O$ = Mean range in $\delta^{18}O$ for that time interval. T range = Temperature range calculated from $\delta^{18}O_c$. Scaled T range = Temperature range multiplied by a scaling factor of 1.55. $\delta^{18}O_{avr}$ = Average $\delta^{18}O_c$ per time period based on resampled but undetrended data. Average T = Average temperature per time period calculated from $\delta^{18}O_{avr}$. The given errors represent one standard deviation.

	Seasonality (detrended $\delta^{18}O_c$ series)			**Averages (undetrended)**	
	$\Delta\delta^{18}O_c$ (‰)	***T range (°C)***	***Scaled T range (°C)***	***$\delta^{18}O_{avr}$ (‰)***	***Average T (°C)***
VB006	0.59 ± 0.15	2.6 ± 0.7	4.0 ± 1.0	2.27 ± 0.13	11.2 ± 0.6
VB020	0.56 ± 0.10	2.4 ± 0.4	3.7 ± 0.7	2.26 ± 0.08	11.3 ± 0.4
VB004+021	0.67 ± 0.16	2.9 ± 0.7	4.5 ± 1.0	2.26 ± 0.17	11.3 ± 0.7
VB023	0.68 ± 0.11	2.9 ± 0.5	4.6 ± 0.7	2.29 ± 0.14	11.1 ± 0.6
3.6 kyr BP avr	**0.65 ± 0.14**	**2.8 ± 0.6**	**4.4 ± 1.0**	**2.27 ± 0.19**	**11.2 ± 0.8**
2003–2013 CE	**0.57 ± 0.14**	**2.5 ± 0.6**	**3.8 ± 1.0**	**2.04 ± 0.07**	**12.2 ± 0.3**

5. Discussion

5.1 Chronology

Seven fossil *G. glycymeris* were crossmatched based on their annual growth patterns, building a floating chronology. Six of the crossmatched shells were later radiocarbon dated, consistently placing all specimens in the 4th millennium BP, thus confirming that they were approximately coeval.

A *G. glycymeris* chronology and annual $\delta^{18}O_c$ series covering the last two centuries have previously been published for the Tiree Passage, Inner Hebrides (Reynolds et al., 2017, 2013). To our knowledge, ours is the first floating bivalve chronology from the Scottish shelf, and the first floating chronology built with *G. glycymeris* shells. Shell lags can contain specimens with age differences of thousands of years (Flessa et al., 1993; Butler et al., 2009). Therefore, it is a time-consuming and often fruitless task to try to crossmatch fossil shells from a shell lag without constraining their ages first. In the present study, there was much trial and error during the construction of the floating chronology, and it is very likely that more shells in the collection were coeval and could have been crossmatched but were missed. Taphonomic factors (i.e. the condition of the shells) do not indicate

for how long shells have been buried in sediment (Butler et al., 2020); instead, radiometric dating is the most common method used to identify whether shells were approximately coeval. However, radiometric dating requires additional resources and is age-limited, and might therefore not always be feasible. While archaeological shell middens may provide more stratigraphic information than shell lags, they usually consist of short-lived species, which are unsuitable for crossmatching (Andrus, 2011). Given these challenges, floating bivalve chronologies remain rare, however, published examples do exist both for shell lags (e.g., Scourse et al., 2006) and shell middens (Helama and Hood, 2011). Finding alternative sampling strategies that help constrain ages in the fossil record has been raised as a priority research question in a recent horizon-scanning survey in the field of sclerochronology (Trofimova et al., 2020).

Due to the lack of long-lived live-collected specimens in the present study, no comparisons between shell growth variability and physical and biological data or climate indices can be made for this location. Several studies have linked shell growth in *G. glycymeris* to SST variability (Brocas et al., 2013; Reynolds et al., 2013; Royer et al., 2013). However, this relationship is likely secondary, since shell growth can be assumed to be primarily influenced by the quality and availability of food (Reynolds et al., 2017). Food availability, in turn, is linked to water circulation and SSTs. At St Kilda, the local food web will likely be affected by upwelling processes (Simpson and Tett, 1986) and the variability in Atlantic vs. shelf water dominance, as different water masses present different chlorophyll distribution patterns (Holligan, 1986) and distinct phytoplankton communities (Aiken et al., 1977).

5.2 The Hebrides Shelf in the fourth millennium BP

The probability distribution in Figure 4 presents a cluster of high-density peaks at 3.7–3.5 cal kyr BP, most likely placing the floating chronology in this time range. This period covers a regional climatic shift on the British Isles from dry to wet conditions, with terrestrial records of this shift grouped around ca. 3.6 cal kyr BP (see Charman, 2010, and references therein). Charman (2010) notes that the wet phase largely coincided with strong solar anomalies and a drop in SSTs south of Iceland at ca. 3.6–3.5 cal kyr BP and 3.4–3.3 cal kyr BP (Berner et al., 2008). Several periods of enhanced precipitation-evaporation (P-E) have been recorded for the British Isles since the mid-Holocene, which are thought to be linked with variability in solar activity and thermohaline circulation (Barber and Charman, 2003; Charman, 2010). However, the role of the ocean in the 3.6 cal kyr BP event is unknown, as evidence for changes in ocean circulation at that time is lacking (Charman, 2010). Charman (2010) hypothesized that this regional P-E shift and the observed decrease in SSTs might have been induced through atmospheric processes alone. In a study on dinocyst

assemblages from the Celtic Sea, Marret et al. (2004) found an increase in oceanic species at 3.6 cal kyr BP, and evidence of decreased seasonality due to milder winters from 3.6 cal kyr BP onwards. These findings would support the hypothesis of stronger westerlies and increased Atlantic inflow on the shelf, which might also have caused wetter conditions on the British Isles (Marret et al., 2004).

5.2.1. Seasonality in the fossil shell record

Because the growth season of *G. glycymeris* does not include winter months, our results do not represent full seasonality. However, the data give an indication of whether the temperature range within the growth season has changed between ca. 3.6 cal kyr BP and today. As shown in Table 2, the seasonal temperature range in the fossil shells were similar to the modern range. Hence, we found no evidence of differences in spring-to-summer seasonality on the Hebrides shelf between the fossil and the modern record.

When investigating past seasonal shelf sea temperatures, possible changes in stratification must be considered. In stratified water, the warm surface layer is separated from the cold bottom layer by the thermocline during the summer. Consequently, the difference between summer SSTs and sea bottom temperatures is higher in stratified water than in vertically mixed water, and summer bottom waters are colder in stratified than in mixed sectors (Elliott et al., 1991). It is therefore essential to know (1) whether the shelf-sea fronts (i.e. fronts between mixed and seasonally stratified waters) have moved position and (2) which depths the fossil material represents. Numerical tidal models and proxy studies have shown that stratification on the NW European shelf started at 10–8 kyr BP and progressed over the following millennia until 6–5 kyr BP (Scourse et al., 2002; Uehara et al., 2006; Ward et al., 2016). The reconstructed temperatures from St Kilda do not indicate that any major change has taken place between the mid-fourth millennium BP and today, which is consistent with data from the Celtic Sea (Austin and Scourse, 1997; Marret et al., 2004; Scourse et al., 2002). Stratification and the evolution of shelf-sea fronts is of high interest as they exert a major influence on primary productivity. Conditions are favourable for productivity along shelf-sea fronts, where both vertical stability and nutrient renewal are given (Pingree et al., 1978). This may in turn affect the growth width chronology, since shell growth is tightly linked to food availability and quality. Due to the local topography at St Kilda, we assume that the fossil shells lived at similar depths as the live-caught specimens, representing a shallow tidally mixed habitat. Sea level change does not have to be considered, as sea level rise in this region has been smaller than 2 m in the last 4,000 years (Gehrels, 2010). Due to the shallow sampling depths, tidal mixing, and the local upwelling system at St Kilda (Simpson and Tett, 1986), we conclude that both the fossil and modern material represent mixed water conditions and are hence more tightly coupled to SSTs and surface air temperature than would be the case if they represented stratified conditions.

5.2.2 Average temperatures in the fossil shell record

Previous studies using summer SST proxies have found evidence of a pronounced cold interval south of Iceland at 4–2 cal kyr BP, while records of this cooling are absent in the Norwegian Sea (e.g., Berner et al., 2008; Orme et al., 2018, and references therein; Van Nieuwenhove et al., 2018). Orme et al. (2018) hypothesize that the colder SSTs might have been caused either by enhanced Arctic outflow or enhanced ice melt from East Greenland, both associated with negative NAO circulation. A weakening of the NAC linked to the low NAO could provide another explanation for the cooling, although this hypothesis is not supported by much evidence (Orme et al., 2018). The reconstructed late spring and summer SSTs for the Hebrides Shelf at ca. 3.7–3.5 cal kyr BP were 1 °C lower than today (2003–2013 CE; Table 2). However, our data do not provide evidence of a distinct cooling event or interval. A major limitation of the present study is the relatively short time interval covered by the fossil isotope record, which does not provide the context of any preceding warmer periods in the mid-Holocene. The temporal context is important, as a warming of ca. 1 °C in annual SSTs has occurred in UK waters over the last 100 years (Hughes et al., 2017). Thus, while the reconstructed temperatures for ca. 3.7–3.5 cal kyr BP are 1 °C cooler than today, they are similar to regional spring and summer SSTs in the early 20th century CE (HadISST reanalysis data; Rayner et al., 2003).

5.3. Sampling techniques and calibration

5.3.1 Instrumental data and limitations of this study

An important and well-known caveat of $\delta^{18}O_c$ temperature reconstructions is that $\delta^{18}O_w$ needs to be known or estimated. The $\delta^{18}O_w$ composition of seawater is controlled by fractionation processes in the hydrological cycle such as evaporation, precipitation, vapour transport, and changes in sea ice; it is thus linked to changes in salinity (Rohling, 2013, and references therein). Furthermore, $\delta^{18}O_w$ varies based on the mixing and advection of water masses with specific $\delta^{18}O_w$ signatures. Large-scale changes in North Atlantic Ocean circulation as well as wind-driven regional processes on the Scottish shelf will contribute to salinity and $\delta^{18}O_w$ variability at St Kilda. However, no local measurements of $\delta^{18}O_w$ are available for either of the two time periods discussed in this study, and no regional salinity–$\delta^{18}O_w$ relationship has yet been formulated. Therefore, we used the $\delta^{18}O_w$ value for surface water from the closest available location in the open ocean and applied it to both the modern and the fossil shell-derived temperature series. At St Kilda, terrestrial freshwater input is negligible and the region was fully deglaciated by the early Holocene (Austin and Kroon, 1996), ruling these factors out as local influences on $\delta^{18}O_w$ variability. Instrumental measurements along the Ellett line since 1975 show that the station closest and most similar to St Kilda (station 15G, Lat: 56.88 °N, Long: 08.50 °W, see

612 Figure 1b), has an average salinity of 35.2 ± 0.2 (Holliday et al., 2015; Jones et al., 2018). How much
613 changes in salinity affect the $\delta^{18}O_w$, and consequently the reconstructed temperature, can be estimated
614 with a salinity–$\delta^{18}O_w$ mixing line. However, as mentioned above, no such mixing line has been
615 developed for the outer western Scottish shelf. Austin et al. (2006) recommend using the equation
616 $\delta^{18}O_w = 0.5972 \times S - 20.6850$ for the Outer Hebrides, which is a modified version of the equation
617 developed by Frew et al. (2000) for the northern North Atlantic. Following this recommendation, a
618 standard deviation of ± 0.2 in salinity would result in a fluctuation of ± 0.5 °C in reconstructed
619 temperature. However, the applicability of this equation to St Kilda remains uncertain, given that St
620 Kilda is influenced both by oceanic and by coastal waters, as well as local dynamics such as cold-
621 water upwelling.

622

623 Another caveat is that there are no *in-situ* temperature measurements available for proxy
624 calibration at our study site. Instrumental hydrographic data are particularly scarce in non-coastal
625 environments like St Kilda. Therefore, gridded satellite data are the best option for calibrating proxy
626 records and tracking changes through time. However, gridded data are spatially smoothed, therefore it
627 is important to have a good understanding of the oceanography of the sample site and choose the grid
628 and kernel size accordingly, to avoid introducing additional error by averaging across different
629 oceanographic regimes. Ideally, the gridded SST datasets should be compared to *in-situ*
630 measurements to ensure that the best-fitting dataset is used for the specific location (see Hughes et al.,
631 2009). Hughes et al. (2009) compared the three products OISST V2 (Reynolds et al., 2002),
632 HadISST1 (Rayner et al., 2003), and ERSST V3 (Smith et al., 2008) to *in-situ* data of six locations in
633 the Northeast Atlantic region. Out of those six locations, the closest and most similar to St Kilda was
634 the Faroe-Shetland channel, where HadISST1 performed best. Boehme et al. (2014) compared the
635 same three gridded datasets to *in-situ* temperature data from the Norwegian Sea and growth data of
636 Atlantic salmon sampled in northern and western Scotland. They recommend OISST V2 for similar
637 studies, or HadISST1 for time series predating 1982. We selected HadISST1 for our study because it
638 performed best in the Faroe-Shetland channel, which is most similar to our sample site (Hughes et al.,
639 2009).

640

641 **5.3.2 Growth season and calibration of modern samples**

642 Microdrilling was the preferred method in this study, as it allows for more control than
643 micromilling and ensures that the samples are all taken from the same portion of the outer shell layer
644 (see section 3.6). Figure 9 shows that the two different sampling techniques yielded similar results.
645 While micromilling provided a higher resolution, it did not always capture the temperature peak. This
646 might be due to time-averaging effects or contamination from the iOSL. Microdrilling was a time-

efficient technique that was used to obtain replicated data across three specimens, for which the averaged (Fig. 8, 9b) and modelled (Fig. 9c) series matched the instrumental temperature peaks in most years. Thus, replication of data was a key factor confirming the accuracy of the results.

It should be noted that the applied sampling techniques will introduce time averaging effects in the $\delta^{18}O_c$ series; hence, the full seasonality captured in the shells might be partially masked in the obtained data. Notwithstanding these averaging effects, our results clearly confirm that $\delta^{18}O_c$ from *G. glycymeris* at St Kilda is a faithful palaeothermometer for seawater temperatures on the Hebrides shelf.

Our results suggest *G. glycymeris* mainly grow their shells from late spring to early or mid-autumn at St Kilda, with greatest growth from May to July/August (Fig. 8, 9). The onset of growth in May coincides with the annual onset of coccolithophore blooms on the outer shelf (Holligan, 1986). Similar growth seasons have been reported for the Tiree Passage (Reynolds et al., 2017) and the Bay of Brest (Featherstone et al., 2020; Royer et al., 2013).
Shell growth in *G. glycymeris* is likely nonlinear, i.e. it varies throughout the growth season (Reynolds et al., 2017). Due to this bias towards certain periods within the growth season, weighted means should be used when reporting average seasonal temperatures (Schöne, 2013). However, due to low sampling resolution as well as insufficient resolution of temperature data, we here instead applied a 6-point cubic spline model to ensure that the data bias in the modern shells and the fossil shells are comparable (Wanamaker et al., 2011).

5.3.3 Comparability of the fossil and modern shells

Raman spectroscopy showed no diagenetic alterations in the fossil shells, and thus the palaeothermometry equation for aragonitic shells applies for the fossil specimens as well. Moreover, the fossil shells were in very good condition (see Fig. 2b,c), indicating that they were buried shortly after death and well preserved. Due to the St Kilda's topographical features described in section 2.2, the fossil shells will most likely have lived at similar depths as the modern samples.

6. Conclusions

We present here a 187-year growth chronology from the fourth millennium BP at St Kilda, western Scotland, based on fossil *G. glycymeris* shells. Sub-annual $\delta^{18}O_c$ records from fossil specimens of the floating chronology and from modern specimens were used to compare growth season and seasonality between the two time periods.

St Kilda is appropriately sited to study the variability of North Atlantic inflow as it is an offshore location close to the shelf margin, with negligible freshwater input. The good fit between gridded SSTs and the $\delta^{18}O_c$-derived *in-situ* temperatures further confirm the applicability of *G. glycymeris* shells from St Kilda as proxies for temperature. However, St Kilda is also influenced by the Scottish Coastal Current and, due to its island topography, local upwelling processes must be considered.

Our results show that the fossil shells experienced a similar growth season and temperature range as the modern shells, which can be attributed to similar boundary conditions in this region. The age uncertainty and short time frame of our $\delta^{18}O_c$ series are limiting factors that prevent conclusions being drawn on the presence or timing of a distinct summer SST cooling event or cold interval. However, the average $\delta^{18}O_c$ of the fossil specimens indicate that late spring and summer SSTs on the Scottish shelf were cooler in the fourth millennium BP than they are today, and comparable to SSTs in the early 20th century. Thus, an extension of the chronology, accompanied by an annually resolved $\delta^{18}O_c$ record, is needed to address the question whether this region was affected by a cold interval. This would also provide more insight into a time that saw a climate shift to wetter conditions on the British Isles, in which the role of the ocean is uncertain. Such an extension of the chronology would be challenging and require additional funding; however, it is feasible.

Acknowledgements

This work was funded by the EU within the framework of the Marie Curie Initial Training Network ARAMACC (project 604802). Micro-Raman spectroscopy was undertaken as part of a rapid access request to the Diamond Light Source (SP13616-1). We thank the crew of the RV *Prince Madog* for the support during the research cruise, and our ARAMACC colleagues for the help with sample collection. Many thanks to Paula J. Reimer, Ron Reimer, and Julia Simpson for hosting SJA at the ^{14}CHRONO Centre, and for the radiocarbon analysis and friendly support. We also thank Paula J. Reimer and two anonymous reviewers for their thoughtful comments that helped improve this manuscript.

References

Aiken, J., Bruce, R.H., Lindley, J.A., 1977. Ecological investigations with the Undulating Oceanographic Recorder: The hydrography and plankton of the waters adjacent to the Orkney and Shetland Islands. Mar. Biol. 39, 77–91.

714 Andrus, C.F.T., 2011. Shell midden sclerochronology. Quat. Sci. Rev. 30, 2892–2905.
715 https://doi.org/10.1016/j.quascirev.2011.07.016

716 Austin, W.E.N., Cage, A.G., Scourse, J.D., 2006. Mid-latitude shelf seas: a NW European perspective
717 on the seasonal dynamics of temperature, salinity and oxygen isotopes. The Holocene 16,
718 937–947. https://doi.org/10.1177/0959683606hl985rp

719 Austin, W.E.N., Kroon, D., 1996. Late glacial sedimentology, foraminifera and stable isotope
720 stratigraphy of the Hebridean Continental Shelf, northwest Scotland, in: Andrews, J.T.,
721 Austin, W.E.N., Bergsten, H., Jennings, A.E. (Eds.), Late Quaternary Palaeoceanography of
722 the North Atlantic Margin. Geol. Soc. Lond. Spec. Publ. 111, pp. 187–213.
723 https://doi.org/10.1144/GSL.SP.1996.111.01.13

724 Austin, W.E.N., Scourse, J.D., 1997. Evolution of seasonal stratification in the Celtic Sea during the
725 Holocene. J. Geol. Soc. Lond. 154, 249–256. https://doi.org/10.1144/gsjgs.154.2.0249

726 Barber, K.E., Charman, D.J., 2003. Holocene palaeoclimate records from peatlands., in: Mackay,
727 A.W., Battarbee, R.W., Birks, H.J.B., Oldfield, F. (Eds.), Global Change in the Holocene.
728 Edward Arnold, London, pp. 210–226.

729 Berner, K.S., Koc, N., Divine, D., Godtliebsen, F., Moros, M., 2008. A decadal-scale Holocene sea
730 surface temperature record from the subpolar North Atlantic constructed using diatoms and
731 statistics and its relation to other climate parameters. Paleobiol. 23.
732 https://doi.org/10.1029/2006PA001339

733 Black, B.A., Andersson, C., Butler, P.G., Carroll, M.L., DeLong, K.L., Reynolds, D.J., Schöne, B.R.,
734 Scourse, J.D., van der Sleen, P., Wanamaker, A.D., Witbaard, R., 2019. The revolution of
735 crossdating in marine palaeoecology and palaeoclimatology. Biol. Lett. 15, 20180665.
736 https://doi.org/10.1098/rsbl.2018.0665

737 Boehme, L., Lonergan, M., Todd, C.D., 2014. Comparison of gridded sea surface temperature
738 datasets for marine ecosystem studies. Mar. Ecol. Prog. Ser. 516, 7–22.
739 https://doi.org/10.3354/meps11023

740 Brinza, L., Schofield, P. F., Mosselmans, J. F. W., Donner, E., Lombi, E., Paterson, D., & Hodson, M.
741 E. (2014) Can earthworm secreted calcium carbonate immobilise Zn in contaminated soils?
742 Soil Biol. and Biochem., 74, 1−10. https://doi.org/10.1016/j.soilbio.2014.01.012

743 Brocas, W.M., Reynolds, D.J., Butler, P.G., Richardson, C.A., Scourse, J.D., Ridgway, I.D., Ramsay,
744 K., 2013. The dog cockle, *Glycymeris glycymeris* (L.), a new annually-resolved
745 sclerochronological archive for the Irish Sea. Palaeogeogr. Palaeoclimatol. Palaeoecol. 373,
746 133–140. https://doi.org/10.1016/j.palaeo.2012.03.030

Bronk Ramsey, C., 2009. Bayesian analysis of radiocarbon dates. Radiocarbon 51, 337–360. https://doi.org/10.2458/azu_js_rc.v51i1.3494

Bronk Ramsey, C., van der Plicht, J., Weninger, B., 2001. 'Wiggle matching' radiocarbon dates. Radiocarbon 43, 381–389. https://doi.org/https://doi.org/10.1017/S0033822200038248

Buckley, M.W., Marshall, J., 2015. Observations, inferences, and mechanisms of the Atlantic Meridional Overturning Circulation: A review. Rev. Geophys. 54, 5–63. https://doi.org/10.1002/2015RG000493.Received

Butler, P.G., Fraser, N.M., Scourse, J.D., Richardson, C.A., Bryant, C., Heinemeier, J., 2020. Is there a reliable taphonomic clock in the temperate North Atlantic? An example from a North Sea population of the mollusc *Arctica islandica*. Palaeogeogr. Palaeoclimatol. Palaeoecol. 560, 109975. https://doi.org/10.1016/j.palaeo.2020.109975

Butler, P.G., Richardson, C.A., Scourse, J.D., Witbaard, R., Schöne, B.R., Fraser, N.M., Wanamaker, A.D., Bryant, C.L., Harris, I., Robertson, I., 2009a. Accurate increment identification and the spatial extent of the common signal in five *Arctica islandica* chronologies from the Fladen Ground, northern North Sea. Paleoceanography 24, PA2210. https://doi.org/10.1029/2008PA001715

Butler, P.G., Scourse, J.D., Richardson, C.A., Wanamaker, A.D., Bryant, C.L., Bennell, J.D., 2009b. Continuous marine radiocarbon reservoir calibration and the ^{13}C Suess effect in the Irish Sea: Results from the first multi-centennial shell-based marine master chronology. Earth Planet. Sci. Lett. 279, 230–241. https://doi.org/10.1016/j.epsl.2008.12.043

Butler, P.G., Wanamaker, A.D., Scourse, J.D., Richardson, C.A., Reynolds, D.J., 2013. Variability of marine climate on the North Icelandic Shelf in a 1357-year proxy archive based on growth increments in the bivalve *Arctica islandica*. Palaeogeogr. Palaeoclimatol. Palaeoecol. 373, 141–151. https://doi.org/10.1016/j.palaeo.2012.01.016

Carré, M., Cheddadi, R., 2017. Seasonality in long-term climate change. Quaternaire 28, 173–177. https://doi.org/10.4000/quaternaire.8018

Charman, D.J., 2010. Centennial climate variability in the British Isles during the mid-late Holocene. Quat. Sci. Rev. 29, 1539–1554. https://doi.org/10.1016/j.quascirev.2009.02.017

Charman, D.J., McCarroll, D., 2010. Climate variability of the British Isles and adjoining seas. Quat. Sci. Rev. 29, 1503–1506. https://doi.org/10.1016/j.quascirev.2010.05.001

Chen, C.-T.A., Huang, T.-H., Chen, Y.-C., Bai, Y., He, X., Kang, Y., 2013. Air–sea exchanges of CO2 in the world's coastal seas. Biogeosciences 10, 6509–6544. https://doi.org/10.5194/bg-10-6509-2013

Cochran, J.K., Kallenberg, K., Landman, N.H., Harries, P.J., Weinreb, D., Turekian, K.K., Beck, A., Cobban, W.A., 2010. Effect of diagenesis on the Sr, O, and C isotope composition of late cretaceous mollusks from the western interior seaway of North America. Am. J. Sci. 310, 69–88. https://doi.org/10.2475/02.2010.01

Cook, E.R., 1985. A time series analysis approach to tree ring standardization. Unpubl. PhD Thesis, University of Arizona, Tucson, USA, pp. 171.

Cook, E.R., Krusic, P.J., 2005. Program ARSTAN: A tree-ring standardization program based on detrending and autoregressive time series modeling, with interactive graphics. Tree-Ring Laboratory Lamont Doherty Earth Observatory of Columbia University Palisades, NY.

Cook, E.R., Shiyatov, S.G., Mazepa, V.S., 1990. Tree-ring standardization and growth-trend estimation, in: Cook, E.R., Kairiukstis, L.A. (Eds.), Methods of dendrochronology: Applications in the environmental sciences. Springer Science+Business Media, Dordrecht, pp. 104–123.

Crippa, G., 2013. The shell ultrastructure of the genus *Glycymeris* Da Costa, 1778: A comparison between fossil and recent specimens. Riv. Ital. Paleontol. Stratigr. 119, 387–399.

Curry, R.G., McCartney, M.S., 2001. Ocean gyre circulation changes associated with the North Atlantic Oscillation. J. Phys. Oceanogr. 31, 3374–3400. https://doi.org/10.1175/1520-0485(2001)031<3374:OGCCAW>2.0.CO;2

De La Pierre, M., Carteret, C., Maschio, L., André, E., Orlando, R., Dovesi, R., 2014. The Raman spectrum of $CaCO_3$ polymorphs calcite and aragonite: A combined experimental and computational study. J. Chem. Phys. 140. https://doi.org/10.1063/1.4871900

Dettman, D., Lohmann, K., 1995. Microsampling carbonates for stable and minor element analysis: Physical separation on a 20 micrometer scale. J. Sediment. Res. A65, 566–569. https://doi.org/10.1306/D426813F-2B26-11D7-8648000102C1865D

Dettman, D.L., Reische, A.K., Lohmann, K.C., 1999. Controls on the stable isotope composition of seasonal growth bands in aragonitic fresh-water bivalves (Unionidae). Geochim. Cosmochim. Acta 63, 1049–1057. https://doi.org/10.1016/S0016-7037(99)00020-4

Doty, M.S., Oguri, M., 1956. The island mass effect. ICES J. Mar. Sci. 22, 33–37. https://doi.org/https://doi.org/10.1093/icesjms/22.1.33

809 Ellett, D.J., Edwards, A., 1983. Oceanography and inshore hydrography of the Inner Hebrides. Proc.
810 R. Soc. Edinburgh 83B, 143–160. https://doi.org/10.1017/S0269727000013385

811 Elliott, A.J., Clarke, T., Li, Z., 1991. Monthly distributions of surface and bottom temperatures in the
812 northwest European shelf seas. Cont. Shelf Res. 11, 453–466. https://doi.org/10.1016/0278-
813 4343(91)90053-9

814 Ellis, J.R., Milligan, S., Readdy, L., South, A., Taylor, N., Brown, M., 2010. MB5301 Mapping
815 spawning and nursery areas of species to be considered in Marine Protected Areas (Marine
816 Conservation Zones). Report No 1: Final Report on development of derived data layers for 40
817 mobile species considered to be of conservation importance.
818 http://randd.defra.gov.uk/Document.aspx?Document=MB5301_9578_FRP.pdf

819 Featherstone, A.M., Butler, P.G., Schöne, B.R., Peharda, M., Thébault, J., 2020. A 45-year sub-annual
820 reconstruction of seawater temperature in the Bay of Brest, France, using the shell oxygen
821 isotope composition of the bivalve *Glycymeris glycymeris*. Holocene 30, 3–12.
822 https://doi.org/10.1177/0959683619865592

823 Flessa, K.W., Cutler, A.H., Meldahl, K.H., 1993. Time and taphonomy: Quantitative estimates of
824 time-averaging and stratigraphic disorder in a shallow marine habitat. Paleobiology 19, 266–
825 286. https://doi.org/10.1017/S0094837300015918

826 Foukal, N.P., Lozier, M.S., 2017. Assessing variability in the size and strength of the North Atlantic
827 subpolar gyre. J. Geophys. Res. Ocean. 122, 6295–6308.
828 https://doi.org/10.1002/2017JC012798

829 Frew, R.D., Dennis, P.F., Heywood, K.J., Meredith, M.P., Boswell, S.M., 2000. The oxygen isotope
830 composition of water masses in the northern North Atlantic. Deep. Res. I 47, 2265–2286.
831 https://doi.org/10.1016/S0967-0637(00)00023-6

832 Füllenbach, C.S., Schöne, B.R., Mertz-Kraus, R. 2015. Strontium/lithium ratio in shells of
833 *Cerastoderma edule* (Bivalvia) – A new potential temperature proxy for brackish
834 environments. Chem. Geol. 417, 341-355. https://doi.org/10.1016/j.chemgeo.2015.10.030

835 Gehrels, W.R., 2010. Late Holocene land- and sea-level changes in the British Isles: Implications for
836 future sea-level predictions. Quat. Sci. Rev. 29, 1648–1660.
837 https://doi.org/10.1016/j.quascirev.2009.09.015

838 Gilbertson, D.D., Schwenninger, J.-L., Kemp, R.A., Rhodes, E.J., 1999. Sand-drift and soil formation
839 along an exposed North Atlantic Coastline: 14,000 years of diverse geomorphological,
840 climatic and human impacts. J. Archaeol. Sci. 26, 439–469.
841 https://doi.org/10.1006/jasc.1998.0360

842 Gonfiantini, R., Stichler, W., Rozanski, K. (1995) Reference and intercomparison materials for stable
843 isotopes of light elements. IAEA TECDOC 825, 67–74.

844 Goodwin, D.H., Flessa, K.W., Schöne, B.R., Dettman, D.L., 2001. Cross-calibration of daily growth
845 increments, stable isotope variation, and temperature in the Gulf of California bivalve mollusk
846 *Chione cortezi*: Implications for paleoenvironmental analysis. Palaios 16, 387.
847 https://doi.org/10.2307/3515578

848 Goslin, J., Fruergaard, M., Sander, L., Gałka, M., Menviel, L., Monkenbusch, J., Thibault, N.,
849 Clemmensen, L.B., 2018. Holocene centennial to millennial shifts in North-Atlantic
850 storminess and ocean dynamics. Sci. Rep. 8, 12778. https://doi.org/10.1038/s41598-018-
851 29949-8

852 Grossman, E.L., Ku, T.-L., 1986. Oxygen and carbon isotope fractionation in biogenic aragonite:
853 Temperature effects. Chem. Geol. (Isotope Geosci. Sect.) 59, 59–74.
854 https://doi.org/10.1016/0168-9622(86)90057-6

855 Hátún, H., Sandø, A.B., Drange, H., Hansen, B., Valdimarsson, H., 2005. Influence of the Atlantic
856 subpolar gyre on the thermohaline circulation. Science 309, 1841–1844.
857 https://doi.org/10.1126/science.1114777

858 Helama, S., Hood, B.C., 2011. Stone Age midden deposition assessed by bivalve sclerochronology
859 and radiocarbon wiggle-matching of *Arctica islandica* shell increments. J. Archaeol. Sci. 38,
860 452–460. https://doi.org/10.1016/j.jas.2010.09.029

861 Holliday, N.P., 2003. Air-sea interaction and circulation changes in the northeast Atlantic. J. Geophys.
862 Res. 108, 1–11. https://doi.org/10.1029/2002jc001344

863 Holliday, N.P., Cunningham, S.A., Johnson, C., Gary, S.F., Griffiths, C., Read, J.F., Sherwin, T.,
864 2015. Multidecadal variability of potential temperature, salinity, and transport in the eastern
865 subpolar North Atlantic. J. Geophys. Res. Ocean. 120, 5945–5967.
866 https://doi.org/10.1002/2015JC010762

867 Holliday, N.P., Hughes, S.L., Bacon, S., Beszczynska-Möller, A., Hansen, B., Lavín, A., Loeng, H.,
868 Mork, K.A., Østerhus, S., Sherwin, T., Walczowski, W., 2008. Reversal of the 1960s to 1990s
869 freshening trend in the northeast North Atlantic and Nordic Seas. Geophys. Res. Lett. 35.
870 https://doi.org/10.1029/2007GL032675

871 Holliday, N.P., Pollard, R.T., Read, J.F., Leach, H., Penny Holliday, N., Pollard, R.T., Read, J.F.,
872 Leach, H., 2000. Water mass properties and fluxes in the Rockall Trough,1975-1998. Deep.
873 Res. 47, 1303–1332. https://doi.org/10.1016/S0967-0637(99)00109-0

Holligan, P.M., 1986. Phytoplankton distributions along the shelf break. Proc. R. Soc. Edinburgh 88B, 239–263. https://doi.org/10.1017/S0269727000004589

Holt, J., Wakelin, S., Huthnance, J., 2009. Down-welling circulation of the northwest European continental shelf: A driving mechanism for the continental shelf carbon pump. Geophys. Res. Lett. 36. https://doi.org/10.1029/2009GL038997

Hughes, S.L., Holliday, N.P., Colbourne, E., Ozhigin, V., Valdimarsson, H., Østerhus, S., Wiltshire, K., 2009. Comparison of *in situ* time-series of temperature with gridded sea surface temperature datasets in the north Atlantic. ICES J. Mar. Sci. 66, 1467–1479. https://doi.org/10.1093/icesjms/fsp041

Hughes, S.L., Holliday, N.P., Gaillard, F., 2012. Variability in the ICES/NAFO region between 1950 and 2009: Observations from the ICES Report on Ocean Climate. ICES J. Mar. Sci. 69, 706–719. https://doi.org/10.1093/icesjms/fss044

Hughes, S.L., Tinker, J., Dye, S., Andres, O., Berry, D.I., Hermanson, L., Hewitt, H., Holliday, N.P., Kent, E.C., Kennington, K., Inall, M., Smyth, T., 2017. Temperature. Mar. Clim. Chang. Impacts Partnersh. Sci. Rev. 22–41. https://doi.org/10.14465/2017.arc10.003.tem

Hut, G. 1987: Consultants group meeting on stable isotope reference samples for geochemical and hydrological investigations, 16–18 September 1985, Vienna. Report to Director General, International Atomic Energy Agency. https://inis.iaea.org/collection/NCLCollectionStore/_Public/18/075/18075746.pdf

Inall, M., Gillibrand, P., Griffiths, C., MacDougal, N., Blackwell, K., 2009. On the oceanographic variability of the North-West European Shelf to the West of Scotland. J. Mar. Syst. 77, 210–226. https://doi.org/10.1016/j.jmarsys.2007.12.012

Jones, D.S., 1983. Sclerochronology: reading the record of the molluscan shell. Am. Sci. 71, 384–391.

Jones, S., Cottier, F., Inall, M., Griffiths, C., 2018. Decadal variability on the Northwest European continental shelf. Prog. Oceanogr. 161, 131–151. https://doi.org/10.1016/j.pocean.2018.01.012

Kennish, M.J., Lutz, R.A., Rhoads, D.C., 1980. Preparation of acetate peels and fractured sections for observation of growth patterns within the bivalve shell, in: Rhoads, D.C., Lutz, R.A. (Eds.), Skeletal Growth of Aquatic Organisms: Biological Records of Environmental Change. Plenum Press, New York, pp. 597–601.

Killam, D.E., Clapham, M.E., 2018. Identifying the ticks of bivalve shell clocks: seasonal growth in relation to temperature and food supply. Palaios 33, 228–236. https://doi.org/10.2110/palo.2017.072

Lynch-Stieglitz, J., Adkins, J.F., Curry, W.B., Dokken, T., Hall, I.R., Herguera, J.C., Hirschi, J.J.-M., Ivanova, E. V, Kissel, C., Marchal, O., Marchitto, T.M., McCave, I.N., McManus, J.F., Mulitza, S., Ninnemann, U., Peeters, F., Yu, E.-F., Zahn, R., 2007. Atlantic meridional overturning circulation during the Last Glacial Maximum. Science 316, 66–69. https://doi.org/10.1126/science.1137127

Marchal, O., Cacho, I., Stocker, T.F., Grimalt, J.O., Calvo, E., Martrat, B., Shackleton, N., Vautravers, M., Cortijo, E., Van Kreveld, S., Andersson, C., Koç, N., Chapman, M., Sbaffi, L., Duplessy, J.C., Sarnthein, M., Turon, J.L., Duprat, J., Jansen, E., 2002. Apparent long-term cooling of the sea surface in the northeast Atlantic and Mediterranean during the Holocene. Quat. Sci. Rev. 21, 455–483. https://doi.org/10.1016/S0277-3791(01)00105-6

Marret, F., Scourse, J., Austin, W., 2004. Holocene shelf-sea seasonal stratification dynamics: a dinoflagellate cyst record from the Celtic Sea, NW European shelf. The Holocene 5, 689–696. https://doi.org/10.1191/0959683604hl747rp

Moffa-Sánchez, P., Born, A., Hall, I.R., Thornalley, D.J.R., Barker, S., 2014. Solar forcing of North Atlantic surface temperature and salinity over the past millennium. Nat. Geosci. 7, 275–278. https://doi.org/10.1038/ngeo2094

Ninnemann, U.S., Thornalley, D.J.R., 2016. Recent natural variability of the Iceland Scotland Overflows on decadal to millennial timescales: Clues from the ooze. US Clivar Var. 14, 1–7.

Olsen, J., Anderson, N.J., Knudsen, M.F., 2012. Variability of the North Atlantic Oscillation over the past 5,200 years. Nat. Geosci. 5, 808–812. https://doi.org/10.1038/ngeo1589

Orme, L.C., Charman, D.J., Reinhardt, L., Jones, R.T., Mitchell, F.J.G., Stefanini, B.S., Barkwith, A., Ellis, M.A., Grosvenor, M., 2017. Past changes in the North Atlantic storm track driven by insolation and sea-ice forcing. Geology 45, 335–338. https://doi.org/10.1130/G38521.1

Orme, L.C., Miettinen, A., Divine, D., Husum, K., Pearce, C., Van Nieuwenhove, N., Born, A., Mohan, R., Seidenkrantz, M.-S., 2018. Subpolar North Atlantic sea surface temperature since 6 ka BP: Indications of anomalous ocean-atmosphere interactions at 4–2 ka BP. Quat. Sci. Rev. 194, 128–142. https://doi.org/10.1016/j.quascirev.2018.07.007

Orme, L.C., Reinhardt, L., Jones, R.T., Charman, D.J., Barkwith, A., Ellis, M.A., 2016. Aeolian sediment reconstructions from the Scottish Outer Hebrides: Late Holocene storminess and the

role of the North Atlantic Oscillation. Quat. Sci. Rev. 132, 15–25. https://doi.org/10.1016/j.quascirev.2015.10.045

Östlund, H.G.; Grall, C., 2001. Part of the global seawater delta oxygen-18 database from reference Östlund 1993. PANGAEA, https://doi.org/10.1594/PANGAEA.58084

Paillard, D., Labeyrie, L., Yiou, P., 1996. AnalySeries 1.0: a Macintosh software for the analysis of geophysical time-series. Eos 77, 379.

Painter, S.C., Hartman, S.E., Kivimae, C., Salt, L.A., Clargo, N.M., Bozec, Y., Daniels, C.J., Jones, S.C., Hemsley, V.S., Munns, L.R., Allen, S.R., 2016. Carbon exchange between a shelf sea and the ocean: The Hebrides Shelf, west of Scotland. J. Geophys. Res. Ocean. 121, 4522–4544. https://doi.org/10.1002/2015JC011599

Parker, J.E., Thompson, S.P., Lennie, A.R., Potter, J., Tang, C.C., 2010. A study of the aragonite-calcite transformation using Raman spectroscopy, synchrotron powder diffraction and scanning electron microscopy. CrystEngComm 12, 1590–1599. https://doi.org/10.1039/B921487A

Pederson, C., Mavromatis, V., Dietzel, M., Rollion-Bard, C., Nehrke, G., Jöns, N., Jochum, K.P., Immenhauser, A., 2019. Diagenesis of mollusc aragonite and the role of fluid reservoirs. Earth Planet. Sci. Lett. 514, 130–142. https://doi.org/10.1016/j.epsl.2019.02.038

Pingree, R.D., Holligan, P.M., Mardell, G.T., 1978. The effects of vertical stability on phytoplankton distributions in the summer on the northwest European Shelf. Deep. Res. 25. https://doi.org/10.1016/0146-6291(78)90584-2

Pingree, R.D., Sinha, B., Griffiths, C.R., 1999. Seasonality of the European slope current (Goban Spur) and ocean margin exchange. Cont. Shelf Res. 19, 929–975. https://doi.org/10.1016/S0278-4343(98)00116-2

Porter, M., Dale, A.C., Jones, S., Siemering, B., Inall, M.E., 2018. Cross-slope flow in the Atlantic Inflow Current driven by the on-shelf deflection of a slope current. Deep. Res. Part I Oceanogr. Res. Pap. 140, 173–185. https://doi.org/10.1016/j.dsr.2018.09.002

Rayner, N. A., Parker, D.E., Horton, E.B., Folland, C.K., Alexander, L. V., Rowell, D.P., Kent, E.C., Kaplan, A., 2003. Global analyses of sea surface temperature, sea ice, and night marine air temperature since the late nineteenth century. J. Geophys. Res. 108, 4407. https://doi.org/10.1029/2002JD002670

Reimer, P.J., Bard, E., Bayliss, A., Beck, W.J., Blackwell, P.G., Bronk Ramsey, C., Buck, C.E., Cheng, H., Edwards, R.L., Friedrich, M., Grootes, P.M., Guilderson, T.P., Haflidason, H.,

Hajdas, I., Hatté, C., Heaton, T.J., Hoffmann, D.L., Hogg, A.G., Hughen, K.A., Kaiser, K.F., Kromer, B., Manning, S.W., Niu, M., Reimer, R.W., Richards, D.A., Scott, E.M., Southon, J.R., Staff, R.A., Turney, C.S.M., van der Plicht, J., 2013. Intcal13 and Marine13 radiocarbon age calibration curves 0–50,000 years cal BP. Radiocarbon 55, 1869–1887. https://doi.org/10.2458/azu_js_rc.55.16947

Reimer, P.J., McCormac, F.G., Moore, J., McCormick, F., Murray, E.V., 2002. Marine radiocarbon reservoir corrections for the mid- to late Holocene in the eastern subpolar North Atlantic. Holocene 12, 129–135. https://doi.org/10.1191/0959683602h1528rp

Reynolds, D.J., Butler, P.G., Williams, S.M., Scourse, J.D., Richardson, C.A., Wanamaker, A.D., Austin, W.E.N., Cage, A.G., Sayer, M.D.J., 2013. A multiproxy reconstruction of Hebridean (NW Scotland) spring sea surface temperatures between AD 1805 and 2010. Palaeogeogr. Palaeoclimatol. Palaeoecol. 386, 275–285. https://doi.org/10.1016/j.palaeo.2013.05.029

Reynolds, D.J., Hall, I.R., Slater, S.M., Scourse, J.D., Halloran, P.R., Sayer, M.D.J., 2017. Reconstructing past seasonal to multicentennial-scale variability in the NE Atlantic Ocean using the long-lived marine bivalve mollusk *Glycymeris glycymeris*. Paleoceanography 32. https://doi.org/ 10.1002/2017PA003154

Reynolds, R.W., Rayner, N.A., Smith, T.M., Stokes, D.C., Wang, W., 2002. An improved *in situ* and satellite SST analysis for climate. J. Clim. 15, 1609–1625. https://doi.org/10.1175/1520-0442(2002)015<1609:AIISAS>2.0.CO;2

Robson, J., Hodson, D., Hawkins, E., Sutton, R., 2014. Atlantic overturning in decline? Nat. Geosci. 7, 2–3. https://doi.org/10.1038/ngeo2050

Rohling, E.J., 2013. Oxygen isotope composition of seawater, in: Elias, S.A. (Ed.), The Encyclopedia of Quaternary Science. Amsterdam: Elsevier, pp. 915–922. https://doi.org/10.1016/B978-0-444-53643-3.00293-4

Ropes, J.W., 1987. Preparation of acetate peels of valves from the ocean quahog, *Arctica islandica*, for age determinations. NOAA Tech. Rep. NMFS 50 1–5.

Royer, C., Thébault, J., Chauvaud, L., Olivier, F., 2013. Structural analysis and paleoenvironmental potential of dog cockle shells (*Glycymeris glycymeris*) in Brittany, northwest France. Palaeogeogr. Palaeoclimatol. Palaeoecol. 373, 123–132. https://doi.org/10.1016/j.palaeo.2012.01.033

Schlitzer, R., 2020. Ocean Data View, http://odv.awi.de

Schmidt, G.A., Bigg, G.R., Rohling, E.J., 1999. Global seawater oxygen-18 database – v1.22. https://data.giss.nasa.gov/o18data/

Schöne, B.R., 2013. *Arctica islandica* (Bivalvia): A unique paleoenvironmental archive of the northern North Atlantic Ocean. Glob. Planet. Change 111, 199–225. https://doi.org/10.1016/j.gloplacha.2013.09.013

Schöne, B.R., Fiebig, J., 2009. Seasonality in the North Sea during the Allerød and Late Medieval Climate Optimum using bivalve sclerochronology. Int. J. Earth Sci. 98, 83–98. https://doi.org/10.1007/s00531-008-0363-7

Schöne, B.R., Fiebig, J., Pfeiffer, M., Gleß, R., Hickson, J., Johnson, A.L.A., Dreyer, W., Oschmann, W., 2005. Climate records from a bivalved Methuselah (*Arctica islandica*, Mollusca; Iceland). Palaeogeogr. Palaeoclimatol. Palaeoecol. 228, 130–148. https://doi.org/10.1016/j.palaeo.2005.03.049

Schöne, B.R., Goodwin, D.H., Flessa, K.W., Dettman, D.L., Roopnarine, P.D., 2002. Sclerochronology and growth of the bivalve mollusks *Chione* (Chionista) *fluctifraga* and *C.* (Chionista) *cortezi* in the northern Gulf of California, Mexico. Veliger 45, 45–54.

Scourse, J., Richardson, C., Forsythe, G., Harris, I., Heinemeier, J., Fraser, N., Briffa, K., Jones, P., 2006. First cross-matched floating chronology from the marine fossil record: data from growth lines of the long-lived bivalve mollusc *Arctica islandica*. The Holocene 16, 967–974. https://doi.org/10.1177/0959683606hl987rp

Scourse, J.D., Austin, W.E.N., Long, B.T., Assinder, D.J., Huws, D., 2002. Holocene evolution of seasonal stratification in the Celtic Sea: Refined age model, mixing depths and foraminiferal stratigraphy. Mar. Geol. 191, 119–145. https://doi.org/10.1016/S0025-3227(02)00528-5

Shapiro, G.I., Hill, A.E., 1997. Dynamics of dense water cascades at the shelf edge. J. Phys. Oceanogr. 27, 2381–2394. https://doi.org/10.1175/1520-0485(1997)027<2381:DODWCA>2.0.CO;2

Shapiro, G.I., Huthnance, J.M., Ivanov, V. V, 2003. Dense water cascading off the continental shelf. J. Geophys. Res. 108. https://doi.org/10.1029/2002JC001610

Simpson, J.H., McCandliss, R.R., 2013. "The Ekman Drain": a conduit to the deep ocean for shelf material. Ocean Dyn. 1063–1072. https://doi.org/10.1007/s10236-013-0644-y

Simpson, J.H., Tett, P.B., 1986. Island stirring effects on phytoplankton growth, in: Bowman, J., Yentsch, M., Peterson, W.T. (Eds.), Tidal Mixing and Plankton Dynamics. Lecture Notes on Coastal and Estuarine Studies. Springer Berlin Heidelberg, pp. 41–76.

1031 Smith, T.M., Reynolds, R.W., Peterson, T.C., Lawrimore, J., 2008. Improvements to NOAA's
1032 historical merged land-ocean surface temperature analysis (1880-2006). J. Clim. 21, 2283–
1033 2296. https://doi.org/10.1175/2007JCLI2100.1

1034 Solignac, S., Grelaud, M., de Vernal, A., Giraudeau, J., Moros, M., McCave, I.N., Hoogakker, B.,
1035 2008. Reorganization of the upper ocean circulation in the mid-Holocene in the northeastern
1036 Atlantic. Can. J. Earth Sci. 45, 1417–1433. https://doi.org/10.1139/E08-061

1037 Souza, A.J., Simpson, J.H., Harikrishnan, M., Malarkey, J., 2001. Flow structure and seasonality in
1038 the Hebridean slope current. Oceanol. Acta 24, 63–76. https://doi.org/10.1016/S0399-
1039 1784(00)01103-8

1040 Steinhilber, F., Abreu, J.A., Beer, J., Brunner, I., Christl, M., Fischer, H., Heikkilä, U., Kubik, P.W.,
1041 Mann, M., McCracken, K.G., Miller, H., Miyahara, H., Oerter, H., Wilhelms, F., 2012. 9,400
1042 years of cosmic radiation and solar activity from ice cores and tree rings. Proc. Natl. Acad.
1043 Sci. U. S. A. 109, 5967–5971. https://doi.org/10.1073/pnas.1118965109

1044 Steinhilber, F., Beer, J., Fröhlich, C., 2009. Total solar irradiance during the Holocene. Geophys. Res.
1045 Lett. 36, L19704. https://doi.org/10.1029/2009GL040142

1046 Stuiver, M., Reimer, P.J., 1993. Extended ^{14}C data base and revised Calib 3.0 ^{14}C age calibration
1047 program. Radiocarbon 35, 215–230.
1048 https://doi.org/https://doi.org/10.1017/S0033822200013904

1049 Sutherland, D.G., Ballantyne, C.K., Walker, M.J.C., 1984. Late Quaternary glaciation and
1050 environmental change on St. Kilda, Scotland, and their palaeoclimatic significance. Boreas
1051 13, 261–272. https://doi.org/10.1111/j.1502-3885.1984.tb01121.x

1052 Swindles, G.T., Lawson, I.T., Matthews, I.P., Blaauw, M., Daley, T.J., Charman, D.J., Roland, T.P.,
1053 Plunkett, G., Schettler, G., Gearey, B.R., Turner, T.E., Rea, H.A., Roe, H.M., Amesbury,
1054 M.J., Chambers, F.M., Holmes, Jonathan, Mitchell, F.J.G., Blackford, J., Blundell, A.,
1055 Branch, N., Holmes, Jane, Langdon, P., McCarroll, J., McDermott, F., Oksanen, P.O.,
1056 Pritchard, O., Stastney, P., Stefanini, B., Young, D., Wheeler, J., Becker, K., Armit, I., 2013.
1057 Centennial-scale climate change in Ireland during the Holocene. Earth-Science Rev. 126,
1058 300–320. https://doi.org/10.1016/j.earscirev.2013.08.012

1059 Taylor, A.H., Stephens, J.A., 1998. The North Atlantic Oscillation and the latitude of the Gulf Stream.
1060 Tellus A 50:1, 134–142. https://doi.org/10.3402/tellusa.v50i1.14517

1061 Thomas, R.D.K., 1975. Functional morphology, ecology, and evolutionary conservatism in the
1062 Glycymerididae (Bivalvia). Palaeontology 18, 217–254.

1063 Trofimova, T., Alexandroff, S.J., Mette, M., Tray, E., Butler, P.G., Campana, S., Harper, E., Johnson,
1064 A.L.A., Morrongiello, J.R., Peharda, M., Schöne, B.R., Andersson, C., Andrus, C.F.T., Black,
1065 B.A., Burchell, M., Carroll, M.L., DeLong, K.L., Gillanders, B.M., Grønkjær, P., Killam, D.,
1066 Prendergast, A.L., Reynolds, D.J., Scourse, J.D., Shirai, K., Thébault, J., Trueman, C., de
1067 Winter, N., 2020. Fundamental questions and applications of sclerochronology: Community-
1068 defined research priorities. Estuar. Coast. Shelf Sci. (in press). doi:
1069 https://doi.org/10.1016/j.ecss.2020.106977.

1070 Trofimova, T., Milano, S., Andersson, C., Bonitz, F.G.W., Schöne, B.R., 2018. Oxygen isotope
1071 composition of *Arctica islandica* aragonite in the context of shell architectural organization:
1072 Implications for paleoclimate reconstructions. Geochemistry, Geophys. Geosystems 19.
1073 https://doi.org/10.1002/2017GC007239

1074 Turrell, W.R., Slesser, G., Payne, R., Adams, R.D., Gillibrand, P.A., 1996. Hydrography of the East
1075 Shetland Basin in relation to decadal North Sea variability. ICES J. Mar. Sci. 53, 899–916.
1076 https://doi.org/10.1006/jmsc.1996.0112

1077 Uehara, K., Scourse, J.D., Horsburgh, K.J., Lambeck, K., Purcell, A.P., 2006. Tidal evolution of the
1078 northwest European shelf seas from the Last Glacial Maximum to the present. J. Geophys.
1079 Res. Ocean. 111, C09025. https://doi.org/10.1029/2006JC003531

1080 Urey, H.C., Lowenstam, H.A., Epstein, S., McKinney, C.R., 1951. Measurement of paleotemperatures
1081 and temperatures of the upper Cretaceous of England, Denmark, and the southeastern United
1082 States. Bull. Geol. Soc. Am. 62, 399–416. https://doi.org/10.1130/0016-
1083 7606(1951)62[399:MOPATO]2.0.CO;2

1084 Van Nieuwenhove, N., Pearce, C., Knudsen, M.F., Røy, H., Seidenkrantz, M.-S., 2018. Meltwater and
1085 seasonality influence on Subpolar Gyre circulation during the Holocene. Palaeogeogr.
1086 Palaeoclimatol. Palaeoecol. 502, 104–118. https://doi.org/10.1016/j.palaeo.2018.05.002

1087 Wanamaker, A.D., Kreutz, K.J., Schöne, B.R., Introne, D.S., 2011. Gulf of Maine shells reveal
1088 changes in seawater temperature seasonality during the Medieval Climate Anomaly and the
1089 Little Ice Age. Palaeogeogr. Palaeoclimatol. Palaeoecol. 302, 43–51.
1090 https://doi.org/10.1016/j.palaeo.2010.06.005

1091 Wanner, H., Beer, J., Bütikofer, J., Crowley, T.J., Cubasch, U., Flückiger, J., Goosse, H., Grosjean,
1092 M., Joos, F., Kaplan, J.O., Küttel, M., Müller, S.A., Prentice, I.C., Solomina, O., Stocker,
1093 T.F., Tarasov, P., Wagner, M., Widmann, M., 2008. Mid- to Late Holocene climate change:
1094 an overview. Quat. Sci. Rev. 27, 1791–1828. https://doi.org/10.1016/j.quascirev.2008.06.013

Ward, S.L., Neill, S.P., Scourse, J.D., Bradley, S.L., Uehara, K., 2016. Sensitivity of palaeotidal models of the northwest European shelf seas to glacial isostatic adjustment since the Last Glacial Maximum. Quat. Sci. Rev. 151, 198–211. https://doi.org/10.1016/j.quascirev.2016.08.034

Wehrmeister, U., Soldati, A. L., Jacob, D. E., Häger, T., & Hofmeister, W. (2010) Raman spectroscopy of synthetic, geological and biological vaterite: a Raman spectroscopic study. J. Raman Spectr., 41, 193–201. https://doi.org/10.1002/jrs.2438

Weidman, C.R., Jones, G.A., Lohmann, K.C., 1994. The long-lived mollusc *Arctica islandica*: A new paleoceanographic tool for the reconstruction of bottom temperatures for the continental shelves of the northern North Atlantic Ocean. J. Geophys. Res. 99, 18,305-18,314. https://doi.org/10.1029/94JC01882

Wigley, T.M.L., Briffa, K.R., Jones, P.D., 1984. On the average value of correlated time series, with applications in dendroclimatology and hydrometeorology. J. Clim. Appl. Meteorol. 23, 201–213. https://doi.org/10.1175/1520-0450(1984)023<0201:OTAVOC>2.0.CO;2